



ORIGINAL RESEARCH

Activated Mesenchymal Stem Cells Induce Recovery Following Stroke Via Regulation of Inflammation and Oligodendrogenesis

Matthew K. Tobin , BSc; Terilyn K. L. Stephen, MSc; Kyra L. Lopez; Melissa R. Pergande, MSc; Amelia M. Bartholomew, MD, MPH; Stephanie M. Cologna, PhD; Orly Lazarov , PhD

BACKGROUND: Brain repair mechanisms fail to promote recovery after stroke, and approaches to induce brain regeneration are scarce. Mesenchymal stem cells (MSC) are thought to be a promising therapeutic option. However, their efficacy is not fully elucidated, and the mechanism underlying their effect is not known.

METHODS AND RESULTS: The middle cerebral artery occlusion model was utilized to determine the efficacy of interferon- γ -activated mesenchymal stem cells (aMSCy) as an acute therapy for stroke. Here we show that treatment with aMSCy is a more potent therapy for stroke than naive MSC. aMSCy treatment results in significant functional recovery assessed by the modified neurological severity score and open-field analysis compared with vehicle-treated animals. aMSCy-treated animals showed significant reductions in infarct size and inhibition of microglial activation. The aMSCy treatment suppressed the hypoxia-induced microglial proinflammatory phenotype more effectively than treatment with naive MSC. Importantly, treatment with aMSCy induced recruitment and differentiation of oligodendrocyte progenitor cells to myelin-producing oligodendrocytes in vivo. To elucidate the mechanism underlying high efficacy of aMSCy therapy, we examined the secretome of aMSCy and compared it to that of naive MSC. Intriguingly, we found that aMSCy but not nMSC upregulated neuron-glia antigen 2, an important extracellular signal and a hallmark protein of oligodendrocyte progenitor cells.

CONCLUSIONS: These results suggest that activation of MSC with interferon- γ induces a potent proregenerative, promyelinating, and anti-inflammatory phenotype of these cells, which increases the potency of aMSCy as an effective therapy for ischemic stroke.

Key Words: inflammation ■ ischemia ■ mesenchymal stem cells ■ oligodendrogenesis ■ stroke ■ therapy

Stroke is the fifth leading cause of death each year in the United States and is the number 1 cause of permanent disability in the world.^{1,2} There are \approx 800 000 new stroke victims in the United States each year, and almost 130 000 mortalities.³ The vast majority, around 90%, of stroke patients suffer from an ischemic stroke caused by temporary or permanent occlusion of a blood vessel to the brain.⁴ Current therapy options for ischemic stroke patients in the acute setting are drastically limited, with only 1 FDA-approved drug, tissue plasminogen activator available. However, because of a number of limitations, mainly a

therapeutic window of 3 to 4.5 hours, only 4% to 7% of patients are eligible for tissue plasminogen activator therapy.⁵ This therapeutic window can be increased to up to 24 hours with the addition of endovascular thrombectomy, but this type of therapy can only be administered in certain hospital settings and only after meeting a number of different treatment criteria.^{6,7} Therefore, it is crucial for new therapeutic options to be developed for the treatment of these patients in the acute setting.

Inflammatory responses after stroke involve both peripheral immune cells and microglia. How these

Correspondence to: Orly Lazarov, PhD, 578 CME (M/C 512), 808 South Wood Street, Chicago, IL 60612. E-mail: olazarov@uic.edu

Supplementary material for this article is available at <https://www.ahajournals.org/doi/suppl/10.1161/JAHA.119.013583>

For Sources of Funding and Disclosures see page 14.

© 2020 The Authors. Published on behalf of the American Heart Association, Inc., by Wiley. This is an open access article under the terms of the Creative Commons Attribution-NonCommercial-NoDerivs License, which permits use and distribution in any medium, provided the original work is properly cited, the use is non-commercial and no modifications or adaptations are made.

JAHA is available at: www.ahajournals.org/journal/jaha

CLINICAL PERSPECTIVE

What Is New?

- Activation of mesenchymal stem cells with interferon- γ promotes proregenerative characteristics and facilitates the anti-inflammatory characteristics of naive mesenchymal stem cells, making them more potent therapy following ischemic stroke.

What Are the Clinical Implications?

- There is an unmet need to develop proregenerative therapy for the treatment of ischemic stroke.
- Most clinical studies using mesenchymal stem cells use them in their naive form, which has limited anti-inflammatory effect and little proregenerative impact.
- Interferon- γ -activated mesenchymal stem cells injected at the acute phase of the insult exhibit both anti-inflammatory and proregenerative effects leading to functional recovery.

OGD	oxygen-glucose deprivation
OPC	oligodendrocyte progenitor cells
PDGFRα	platelet-derived growth factor receptor α
SVZ	subventricular zone
TNF-α	tumor necrosis factor α

Nonstandard Abbreviations and Acronyms

7-AAD	7-aminoactinomycin D
aMSCy	interferon- γ -activated mesenchymal stem cells
BDNF	brain-derived neurotrophic factor
BMP1	bone morphogenetic protein 1
CNPase	2',3'-cyclic-nucleotide 3'-phosphodiesterase
CSPG4	chondroitin sulfate proteoglycan 4
DCX	doublecortin
DIC	differential interference contrast
GDNF	glial cell-derived neurotrophic factor
GFAP	glial fibrillary acidic protein
IFN-γ	interferon- γ
IGF-1	insulin-like growth factor 1
IL-4	interleukin 4
IL-6	interleukin 6
LDH	lactate dehydrogenase
MBP	myelin basic protein
MCAO	middle cerebral artery occlusion
MG	microglia
MRI	magnetic resonance imaging
MSC	mesenchymal stem cells
MTT	3-(4,5-dimethylthiazol-2-yl)-2,5-diphenyltetrazolium bromide
N.D.	not detected
nMSC	naive mesenchymal stem cells
NPC	neural progenitor cell(s)
NSC	neural stem cell(s)

processes affect long-term brain repair is still not fully understood. Many studies have demonstrated both detrimental^{18,9} and beneficial¹⁰⁻¹² effects of brain inflammation. Furthermore, these changes, and whether they are good or bad, often depend on the time frame in which they are studied, with the beneficial effects of these cells attributed to the chronic phase of stroke.¹³⁻¹⁵ There have been numerous research studies and clinical trials looking into the efficacy of anti-inflammatory agents as stroke therapies; however, the majority of these studies reported either worse outcomes or no change from placebo,¹⁶ and all failed to make it beyond clinical trials.

Endogenous neurogenesis processes, long posited as therapeutic targets for brain repair, have largely been noncontributory in the setting of ischemic stroke. Although endogenous neural stem cells (NSC) do react acutely to ischemic stroke with increases in cell proliferation and cell migration,¹⁷⁻²² only 10% to 20% of these cells survive long term.^{18,23} These few surviving cells, however, do seem to mature into functional cells,^{18,24,25} with the majority of them becoming spiny neostriatal projection neurons^{18,24} or calretinin-positive interneurons.²⁶ But despite these interesting data, it is still largely unknown why the vast majority of these new cells do not mature and survive long term and why they fail to support brain recovery.

Mesenchymal stem cells (MSC) have unique characteristics that make them an interesting tool to study brain repair after ischemic stroke. They have the ability to (1) reduce overall inflammation, thereby eliminating the potentially toxic environment that could be leading to NSC death,²⁷⁻²⁹ and (2) help support NSC survival and function via secretion of various neurotrophic factors.²⁹⁻³² To date, there have been many preclinical studies as well as clinical trials demonstrating the efficacy of MSC therapy in stroke preclinical studies and safety of MSC treatment in clinical trials.³³⁻⁴⁷ Nevertheless, the extent of recovery following MSC treatment is not clear. Importantly, the mechanism by which MSC treatment conveys a functional benefit is not known, which impedes the development of an effective therapy. Additionally, most of the clinical trials using MSC have utilized this treatment in subacute^{39,48-50} and chronic⁵¹⁻⁵⁵ stroke patients. Therefore, whether these cells can be an effective therapy acutely is largely unknown. Additionally, previous graft-versus-host studies

have demonstrated that when MSC are activated by interferon- γ (IFN- γ) ex vivo (aMSCy), their effect is greatly enhanced, and similar effect sizes can be seen using substantially fewer cells.^{56,57} However, the efficacy of aMSCy in brain repair is unknown.

In these studies we examined whether treatment with aMSCy acutely after ischemic stroke could enhance functional recovery and compared its efficacy and mechanism to treatment with naive MSC (nMSC). In addition, we investigated how microglia and NSC responded to hypoxia and ischemia and how treatment with aMSCy could regulate these cell types to promote long-term functional recovery after stroke. Finally, we analyzed the secretome of aMSCy and nMSC in an attempt to determine the factors underlying the extent of functional recovery that these treatments exert.

METHODS

Detailed materials and methods can be found in Data S1. Data sets generated or analyzed for these studies are available from the corresponding author upon reasonable request. Mass spectrometry proteomics data have been deposited to the ProteomeXchange Consortium via the MassIVE repository with the dataset identifier HYPERLINK "ftp://massive.ucsd.edu/MSV000082984" MSV000082984. Figure 6 and Supplemental Tables 3 and 4 were generated from these data.

Study Design

For all studies, sample sizes were predetermined using published data and our previous studies using G*Power 3.1 (Department of Psychology, Heinrich Heine Universität, Düsseldorf, Germany)⁵⁸ assuming a 2-sided α level of 0.05, power of 80%, and homogeneous variances. Before the beginning of experiments, animals were randomly assigned to groups using a random number generator. Investigators responsible for data collection and analyses were blinded to group allocation throughout the experiments. End points were determined in advance as 24 hours, 1 week, or 3 weeks after reperfusion or for humane end points as determined by our institutional animal care and use committee. No data were excluded from these studies, and no outliers are reported.

Animals

All animal experiments were approved by the University of Illinois at Chicago Institutional Animal Care and Use Committee and are reported according to the ARRIVE (Animal Research Reporting of In Vivo Experiments) guidelines. For surgical experiments female Sprague-Dawley rats (age 14-16 weeks,

weight 225-275 g) were purchased from Envigo (Huntingdon, Cambridgeshire, UK) and were group housed and maintained in standard housing conditions (14/10 hour light/dark cycle) with access to food and water ad libitum. Postoperatively, the animals were singly housed.

Middle Cerebral Artery Occlusion

Focal cerebral ischemia was induced using the middle cerebral artery occlusion model (MCAO) as detailed previously.⁵⁹ Briefly, anesthesia was induced and maintained in isoflurane in 100% oxygen for the duration of the procedure, and body temperature was maintained at $37\pm 0.4^\circ\text{C}$ via rectal probe-monitored heating pad. Ventral midline neck dissection was performed, and the right middle cerebral artery was occluded via intraluminal filament for 90 minutes before the filament was removed, and the animal was allowed to recover. The model is described in detail in Data S1. Three hours following the onset of reperfusion after MCAO, the animals were reanesthetized with isoflurane, and MSC were administered intravenously via the retro-orbital sinus. Cells were given at a dose of 5×10^6 cells/kg.

Behavioral Testing After MCAO

Animals were scored using the modified neurological severity score obtained at baseline before surgery and on postoperative days 1 to 7, 14, and 21, with higher scores reflecting worse impairment. Animals were also subjected to open-field testing for 15 minutes on postoperative days 1 and 7 using an open-field apparatus (Med Associates, Inc, Fairfax, VT). Center/periphery analysis and rotational analysis were done using predetermined configurations in the corresponding Activity Monitor Software package (Med Associates, Inc).

Magnetic Resonance Imaging

Image Acquisition

Forty-eight hours after surgery, animals were anesthetized using isoflurane, and magnetic resonance imaging was performed using an Agilent 9.4T magnetic resonance system (Agilent Technologies, Santa Clara, CA) with a 600 mT/m gradient insert, a 72-mm inside diameter active decoupling birdcage radiofrequency coil for transmission, and a 4-channel phase-array coil as the receiver (Rapid Biomed, Rippar, Germany). In each animal T1-, T2-, and diffusion-weighted magnetic resonance images were acquired using spin-echo multislice sequences. For the T1 sequence, imaging settings were as follows: TR/TE=555/13 ms, field of view=40 \times 40 mm, averages=6, matrix=256 \times 256, slice thickness=1.0 mm, gap=0 mm. For the T2 sequence,

imaging settings were as follows: TR/TE=2000/45 ms, field of view=40×40 mm, averages=4, matrix=256×256, slice thickness=1.0 mm, gap=0 mm. For the diffusion-weighted imaging sequence, imaging settings were as follows: TR/TE=2000/45 ms, field of view=40×40 mm, averages=2, matrix=128×128, slice thickness=1.0 mm, gap=0 mm, 2 b-values of 0 and 650 s/mm², diffusion separation Δ=25 ms, diffusion gradient duration δ=5 ms.

Infarct Volume Calculation

Infarct volume and percentage infarction were calculated using the diffusion-weighted magnetic resonance imaging (MRI) sequences. With correction for edema, these were calculated as follows:

$$\text{Infarct volume (mm}^2\text{)} = \sum_1^n \ln V_n - (\text{Ip}V_n - \text{Co}V_n)$$

$$\text{Percent infarction (\%)} = 100 \times \frac{\sum_1^n \ln V_n}{\sum_1^n (\text{Ip}V_n + \text{Co}V_n)}$$

where the individual slice infarct volume is $\ln V$, the individual slice ipsilateral hemisphere volume is $\text{Ip}V$, individual slice contralateral hemisphere volume is $\text{Co}V$, and n is the slice number.

MSC Isolation and Culture

Female rats <4 weeks of age were euthanized via isoflurane overdose and decapitation. Femurs and tibias were dissected out, and bone marrow plugs were flushed out of the bones. The cell suspension was washed, filtered through a 70-μm cell strainer, spun, resuspended in warm growth medium, and plated at 37°C plus 5% CO₂. Medium was changed after 24 hours and every 3 days thereafter. MSC were purified via magnetic bead negative selection using anti-CD11b and anti-CD45 antibodies to remove contaminating macrophages, and phenotype was confirmed via flow cytometry. Detailed methodologies are described in Data S1. For in vitro activation with IFN-γ, MSC were plated at a density of 3000 cells/cm² and supplemented with 500 U/mL recombinant rat IFN-γ on days 0 and 3 of plating. Cells were used on day 6 after plating. To collect MSC-conditioned medium, MSC were plated at a density of 3000 cells/cm² and were cultured normally or treated with IFN-γ as above. On day 6 after plating, media were removed, cells were washed 3 times, and appropriate media were added. After 24 hours, media were collected, spun at 300g for 10 minutes to remove cell debris, and filtered through a 0.22-μm syringe filter. Media were either used immediately or frozen at -80°C for use at a later time.

Statistical Analyses

All statistical analyses were done in GraphPad Prism (Version 7.03; GraphPad Software Inc, San Diego, CA). All data shown represent mean±SEM, and a probability of <0.05 was considered statistically significant. Data were analyzed with nonparametric testing where appropriate. Individual statistical analyses are described in the appropriate text and figure legends.

RESULTS

MSC Improve Functional Recovery Following MCAO

We set out to determine whether nMSC or aMSCy could be beneficial in treating ischemic stroke acutely. To do this, rats were subjected to 90 minutes of MCAO, administered vehicle (saline), nMSC, or aMSCy intravenously 3 hours after reperfusion, assessed using open-field testing and modified neurological severity score,⁶⁰ and had MRI performed to assess lesion sizes. We found that vehicle-treated stroke animals performed worse during open-field testing compared with sham animals (Figure 1A and 1B) and that both nMSC (Figure 1C) and aMSCy treatments (Figure 1D) caused complete functional recovery. At 24 hours, we show that vehicle-treated animals had traveled less distance (Figure 1E), for fewer times (Figure 1F), and for less time (Figure 1G) than did sham animals, and both nMSC and aMSCy treatment corrected all of these metrics. Furthermore, all animals moved at the same velocity (Figure 1H), suggesting that the impairments in the vehicle-treated animals are not an inability to initiate movement but rather an inability to sustain ambulation. Further, although not significant, vehicle-treated animals had a trending preference for turning in a clockwise fashion (Figure 1I; a manifestation of unilateral brain injury) compared with sham animals, with MSC treatment eliminating this preference. These changes were maintained 7 days after surgery (Figure 1J through 1N).

Additionally, when assessed via modified neurological severity score, animals treated with both nMSC and aMSCy exhibited a more rapid recovery, with animals returning to near baseline functional status by day 21 (Figure 1O). Although vehicle-treated animals did improve significantly from day 1 to day 21, they still remained significantly more impaired compared with MSC-treated animals, and there were no differences between nMSC- and aMSCy-treated animals. Last, MRI imaging was performed (Figure 1P and Video S1) to quantify lesion sizes in these animals. Both nMSC- and aMSCy-treated animals had significantly smaller infarct volumes (Figure 1Q) and percentage infarction (Figure 1R) compared with vehicle-treated animals,

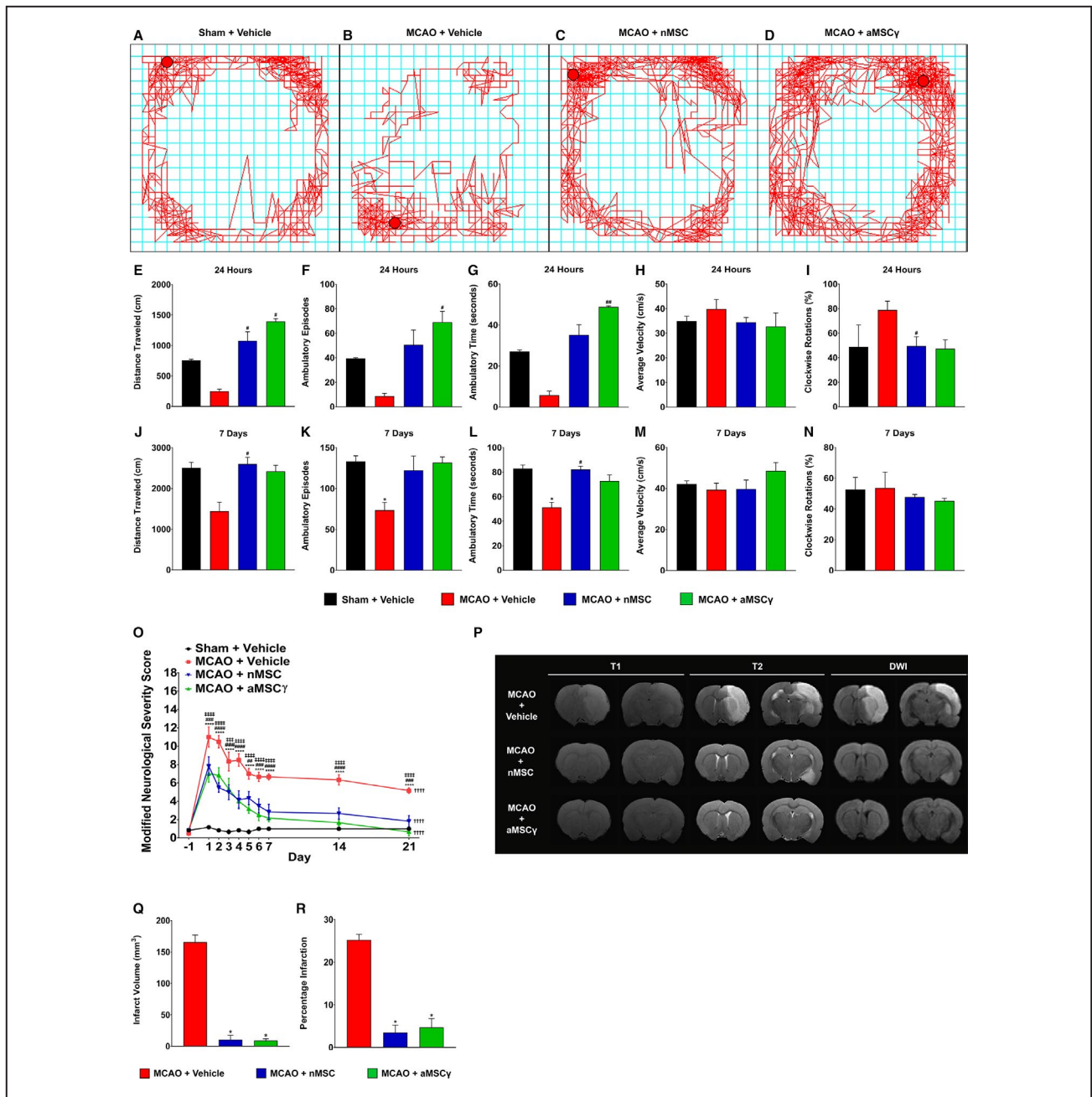


Figure 1. Mesenchymal stem cells (MSC) improve functional recovery and infarct volume following middle cerebral artery occlusion (MCAO).

A through **D**, Representative open field line tracking of sham+vehicle (**A**), MCAO+vehicle (**B**), MCAO+nMSC (**C**), and MCAO+aMSC γ (**D**). **E** through **I**, Open-field measures from sham+vehicle (black), MCAO+vehicle (red), MCAO+nMSC (blue), and MCAO+aMSC γ (green) animals of total distance traveled (**E**), ambulatory episodes (**F**), ambulatory time (**G**), average velocity (**H**), and clockwise rotations (**I**) 24 hours after surgery and treatment. **J** through **N**, Open-field measures of total distance traveled (**J**), ambulatory episodes (**K**), ambulatory time (**L**), average velocity (**M**), and clockwise rotations (**N**) 7 days after surgery and treatment. Data are mean \pm SEM; n=3 animals per group. Data were compared using nonparametric Kruskal-Wallis 1-way ANOVA. *Compared with Sham+Vehicle. #Compared with MCAO+Vehicle. * $P \leq 0.05$, # $P \leq 0.05$, ## $P < 0.01$. **O**, Modified neurological severity score of sham+vehicle (black), MCAO+vehicle (red), MCAO+nMSC (blue), and MCAO+aMSC γ (green) animals. Data were compared using repeated-measures 2-way ANOVA with Holm-Sidak multiple-comparison testing. *Sham+Vehicle vs MCAO+Vehicle; #MCAO+Vehicle vs MCAO+nMSC; †MCAO+Vehicle vs MCAO+aMSC γ ; †Day 1 vs Day 21. ** $P < 0.01$, *** $P < 0.001$, **** $P < 0.0001$, ## $P < 0.01$, ### $P < 0.001$, #### $P < 0.0001$, ††† $P < 0.0001$, †††† $P < 0.0001$, ††††† $P < 0.0001$. **P**, Representative T1-weighted, T2-weighted, and diffusion-weighted imaging (DWI) from MCAO+vehicle (top), MCAO+nMSC (middle), and MCAO+aMSC γ (bottom) animals 48 hours after surgery. **Q**, Infarct volume calculations from MCAO+vehicle (red), MCAO+nMSC (blue), and MCAO+aMSC γ (green) animals. **R**, Percentage infarction calculations from MCAO+vehicle (red), MCAO+nMSC (blue), and MCAO+aMSC γ (green) animals. Data are mean \pm SEM; n=3 animals per group. Data were compared using nonparametric Kruskal-Wallis 1-way ANOVA. * $P \leq 0.05$. aMSC γ indicates interferon- γ -activated mesenchymal stem cells; and nMSC, naive mesenchymal stem cells.

and sham animals demonstrated no lesion on MRI (data not shown).

MSC Reduce Microglia Activation and Inflammatory Signaling

A large portion of damage done following a stroke is a result of inflammatory mediators released by immune cells, especially activated microglia. This response results in an increase in toxic inflammatory mediators including but not limited to interleukin-1 β (IL-1 β), IL-6, and tumor necrosis factor- α (TNF- α).⁶¹ MSC have been demonstrated to preferentially polarize peripheral macrophages to a proregenerative phenotype as well as to reduce secreted levels of IL-12 and TNF- α and increase secretion of the proregenerative IL-10.⁶² Furthermore, it has been shown that in a mouse model of wound healing, both nMSC and, to a greater extent, aMSCy MSC enhance regeneration and wound healing demonstrated by increased wound tensile strength, with this effect being abrogated by depletion of macrophages.⁵⁷ However, how MSC affects microglia following a stroke is not fully elucidated. Microglia are specialized cells originating from a hematopoietic lineage,^{63,64} similar to macrophages, and we hypothesized that these interactions between macrophages and MSC would hold. To investigate this, brain sections from vehicle-treated, nMSC-treated, and aMSCy-treated rats were evaluated for cluster of differentiation 68 (CD68) immunoreactivity 1 week after MCAO (Figure 2A through 2C). CD68 is highly expressed in the monocyte lineage.⁶⁵ We found that animals treated with both nMSC and aMSCy had reduced immunoreactivity for CD68 (Figure 2D) compared with vehicle-treated animals, with sham animals demonstrating no CD68 immunoreactivity (for the latter, data not shown). Furthermore, when assessed at 3 weeks after MCAO, nMSC- and aMSCy-treated animals maintained reductions in CD68 immunoreactivity (Figure 2F and 2G) compared with vehicle-treated animals (Figure 2E). Interestingly, at the 3-week time point, brains from vehicle-treated animals had undergone liquefactive necrosis with demonstration of a large cavity lesion (Figure 2E, outlined by dashed white line), which was not present in nMSC- and aMSCy-treated animals (Figure 2F and 2G). In addition to quantifying total CD68 immunoreactivity, we also analyzed microglia morphology in the peri-infarct region from vehicle-treated (Figure 2H,H'), nMSC-treated (Figure 2I,I'), and aMSCy-treated animals (Figure 2J,J') and found, that in vehicle-treated animals, microglia had morphologies consistent with activated microglia with large cell bodies and few processes, whereas microglia from MSC-treated

animals exhibited morphology much more consistent with resting-state microglia with small cell bodies and numerous branching processes.

To further characterize how microglia respond to MSC treatment following hypoxia, primary microglia were primed in oxygen- and glucose-deprivation conditions (OGD) and then cultured in normal medium, conditioned medium from nMSC, or conditioned medium from aMSCy. We found that when cultured in both nMSC- and aMSCy-conditioned media, microglia have reduced secretion of proinflammatory cytokines IL-6 (Figure 2K) and TNF- α (Figure 2L) 48 hours later. Additionally, although not detectable in cells grown in normal medium, levels of anti-inflammatory IL-4 (Figure 2M) and IL-10 (Figure 2N) were detected at 7 days in cells grown in MSC-conditioned media, with aMSCy having the largest effect. These data show that, similar to previous studies with peripheral macrophages, MSC have the ability to reduce microglial activation as well as convert them from a proinflammatory phenotype to a proregenerative phenotype. To validate the effect of hypoxia on cytokine production by microglia, we subjected primary microglial-cultured cells to OGD. Secreted levels of IL-6 and TNF- α (Figure 2O and 2P, respectively) were significantly increased 48 hours after OGD compared with levels at 24 hours. To determine whether alterations in cytokine production following OGD were the result of the increased number of cells, we examined the viability as well as the toxicity levels in culture using MTT [3-(4,5-dimethylthiazol-2-yl)-2,5-diphenyltetrazolium bromide], LDH (lactate dehydrogenase), and terminal deoxynucleotidyl transferase dUTP nick end labeling assays. We observed some reduction in viability based on the MTT assay but no sign of toxicity or apoptosis in the culture (Figures S1 and S2). These results support the notion that MSC reverse the effect of hypoxia on microglial phenotype following stroke.

aMSCy Induce Oligodendrogenesis Following MCAO

Another cell population that plays a role following stroke are neural progenitor cells (NPC) in the subventricular zone (SVZ). An estimated 10% of NPC survive after stroke.²³ Hypotheses demonstrating the detrimental effects of inflammation on neurogenesis have been proposed.^{8,9} However, how inflammatory mediators released by immune cells, especially activated microglia, affect NSC and NPC is still largely unknown. To start to address that, we quantified the extent of cell proliferation and lineage markers in both the ipsilateral SVZ and ipsilateral striatum (Figure 3). We found that 24 hours after MCAO, vehicle-treated animals had a reduced number of proliferating cells, whereas aMSCy-treated rats had similar number of proliferating cells to sham animals (Figure 3A through

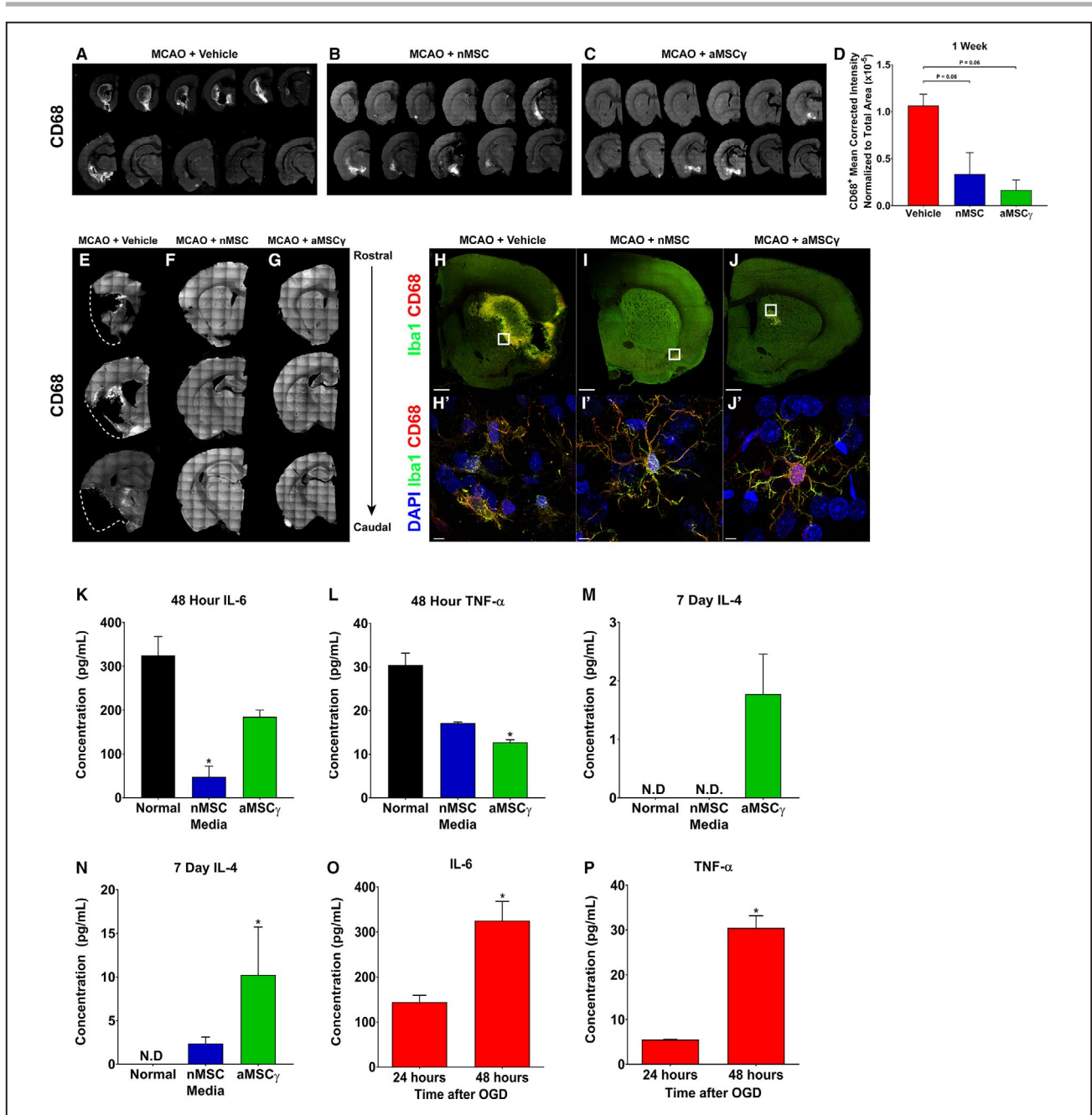


Figure 2. Mesenchymal stem cells (MSC) reduce microglia activation and inflammatory signaling.

A through C, Representative images of CD68 staining of brain sections spaced 300 μm apart through the whole brain from middle cerebral artery occlusion (MCAO)+vehicle (**A**), MCAO+nMSC (**B**), and MCAO+aMSC_γ (**C**) animals 1 week after surgery and treatment. **D,** Quantitation of CD68 staining 1 week after surgery and treatment. Data are mean±SEM; n=3 to 4 animals per group. Data were analyzed using nonparametric Kruskal-Wallis 1-way ANOVA. **E through G,** Representative images of CD68 staining of brain sections spaced 300 μm apart through the whole brain from MCAO+vehicle (**E**), MCAO+nMSC (**F**), and MCAO+aMSC_γ (**G**) animals 3 weeks after surgery and treatment. Dashed lines (**E**) approximate the location of the lateral border of the tissue in a normal brain. **H through J,** Representative confocal images of whole brain slices of MCAO+vehicle (**H**), MCAO+nMSC (**I**), and MCAO+aMSC_γ (**J**) animals 1 week after surgery and treatment stained for Iba1 (green) and CD68 (red). Scale bar represents 1 mm. **H' through J',** Representative confocal images at high magnification from the white boxes in **H through J** stained for DAPI (blue), Iba1 (green), and CD68 (red). Scale bar represents 5 μm. **K through N,** Concentration of interleukin 6 (IL-6) (**K**), tumor necrosis factor α (TNF-α) (**L**), IL-4 (**M**), and IL-10 (**N**) secreted by primary microglia after priming in oxygen and glucose deprivation (OGD) and then growth in normal (black), nMSC-conditioned medium (blue), or aMSC_γ conditioned medium (green). IL-6 and TNF-α were assayed at 48 hours, and IL-4 and IL-10 were assayed at 7 days. Data are mean±SEM; n=3 independent experiments. Data were analyzed using a nonparametric Kruskal-Wallis 1-way ANOVA. N.D., not detected, *Compared with Normal, *P≤0.05. **O and P,** Concentration of IL-6 (**O**) and TNF-α (**P**) secreted by primary microglia after OGD. Data are mean±SEM; n=3 independent experiments. Data were analyzed using a 2-tail, unpaired t test. *P≤0.05. aMSC_γ indicates interferon-γ-activated mesenchymal stem cells; and nMSC, naive mesenchymal stem cells.

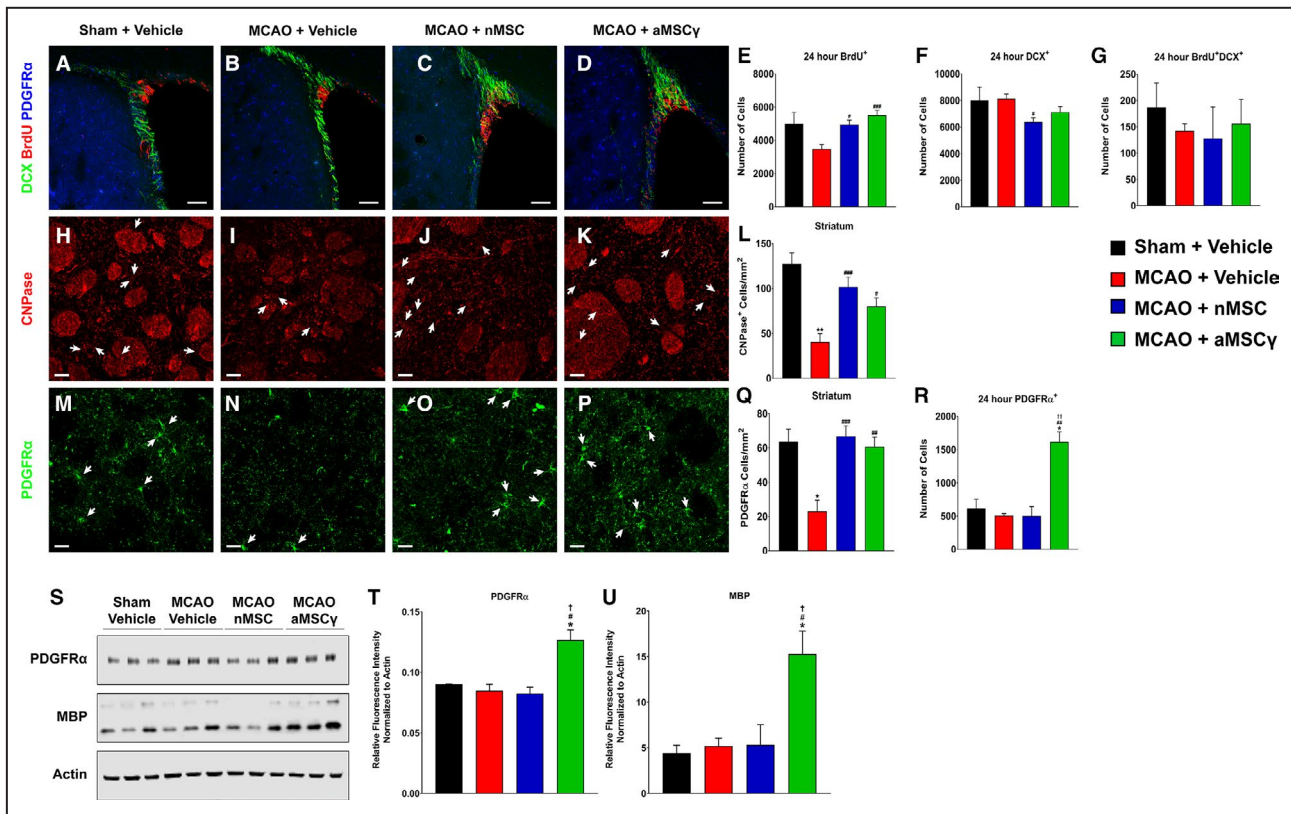


Figure 3. Interferon- γ -activated mesenchymal stem cells (aMSCy) induce oligodendrogenesis following middle cerebral artery occlusion (MCAO).

A through **D**, Representative confocal images of the ipsilateral SVZ from sham+vehicle (**A**), MCAO+vehicle (**B**), MCAO+nMSC (**C**), and MCAO+aMSCy (**D**) animals 24 hours after surgery and treatment stained for doublecortin (DCX, green), bromodeoxyuridine (BrdU, red), and platelet-derived growth factor receptor α (PDGFR α , blue). Scale bar represents 100 μ m. **E** through **G**, Quantification of total numbers of BrdU $^+$ cells (**E**), DCX $^+$ cells (**F**), and BrdU $^+$ DCX $^+$ cells (**G**) in the ipsilateral SVZ 24 hours after MCAO. Data are mean \pm SEM; n=3 animals for the sham group and n=5 to 6 animals for the remaining groups. Data were analyzed using nonparametric Kruskal-Wallis 1-way ANOVA. *Compared with sham+vehicle. #Compared with MCAO+vehicle. * P \leq 0.05, # P \leq 0.05. **H** through **K**, Representative confocal images of the ipsilateral striatum from sham+vehicle (**H**), MCAO+vehicle (**I**), MCAO+nMSC (**J**), and MCAO+aMSCy (**K**) animals 3 weeks after surgery and treatment stained for 2'3'-cyclic-nucleotide 3'-phosphodiesterase (CNPase, red). Scale bar represents 20 μ m. **L**, Quantification of CNPase $^+$ cells in the ipsilateral striatum. Data are mean \pm SEM; n=3 animals per group. Data were analyzed using nonparametric Kruskal-Wallis 1-way ANOVA. *Compared with sham+vehicle. #Compared with MCAO+vehicle. ** P \leq 0.01, # P \leq 0.05, ### P \leq 0.001. **M** through **P**, Representative confocal images of the ipsilateral striatum from sham+vehicle (**M**), MCAO+vehicle (**N**), MCAO+nMSC (**O**), and MCAO+aMSCy (**P**) animals 3 weeks after surgery and treatment stained for PDGFR α (green). Scale bar represents 20 μ m. **Q**, Quantification of PDGFR α $^+$ cells in the ipsilateral striatum. Data are mean \pm SEM; n=3 animals per group. Data were analyzed using nonparametric 1-way Kruskal-Wallis ANOVA. *Compared with sham+vehicle. #Compared with MCAO+vehicle. * P \leq 0.05, ## P \leq 0.01, ### P \leq 0.001. **R**, Quantification of total numbers of PDGFR α $^+$ cells in the ipsilateral subventricular zone (SVZ) 24 hours after MCAO. Data are mean \pm SEM; n=3 animals for the sham group and n=5 to 6 animals for the remaining groups. Data were analyzed using nonparametric Kruskal-Wallis 1-way ANOVA. *Compared with sham+vehicle. #Compared with MCAO+vehicle. †Compared with MCAO+nMSC. * P \leq 0.05, ## P \leq 0.01, †† P \leq 0.01. **S** through **U**, Western blots of the oligoprogenitor marker PDGFR α and mature oligodendrocyte marker MBP (myelin basic protein) (**S**) and their quantification (**T** and **U**) from brain homogenate from the ipsilateral hemisphere 1 week after surgery and treatment normalized to actin. Data are mean \pm SEM; n=3 animals per group. Data were analyzed using nonparametric Kruskal-Wallis 1-way ANOVA. *Compared with sham+vehicle. #Compared with MCAO+vehicle. †Compared with MCAO+nMSC. * P \leq 0.05, # P \leq 0.05, † P \leq 0.05. nMSC indicates naive mesenchymal stem cells.

3E). Further, after MCAO, vehicle-treated animals had no changes in the number of neuroblasts/immature neurons (Figure 3F). No change was observed in the number of proliferating neuroblasts (Figure 3G). This suggests that the increase in the number of proliferating cells observed in the MSC-treated animals does not lead to an increased number of cells differentiating into neurons. Thus, we asked whether proliferating

cells differentiate into other cell types. For this purpose we examined the number of cells expressing platelet-derived growth factor receptor α (PDGFR α). These precursors give rise to myelin-producing oligodendrocytes.⁶⁶ Interestingly, we observed a marked increase in the number of cells in the oligodendrocytic lineage in the SVZ of aMSCy-treated rats compared with sham, vehicle-, or nMSC-treated MCAO rats (Figure 3H

through 3R). The significant increase in the number of PDGFR α -positive cells in the SVZ of aMSCy-treated rats suggested that aMSCy induce an oligodendrogenic phenotype (Figure 3R).

These changes, however, were not sustained 1 week after MCAO (Figure S3). Additionally, when examining SVZ cell counts 3 weeks after MCAO, we found significant decreases in the numbers of neuroblasts/immature neurons (Figure S4A and S4B) with no changes in the number of mature oligodendrocytes in the SVZ (Figure S4C). This suggests that the increase in oligodendrocyte progenitors at 24 hours contributes to cells migrating out of the SVZ into the striatum toward the ischemic lesion. To investigate this, we assessed numbers of mature oligodendrocytes and oligodendrocyte progenitor cells in the ipsilateral striatum. We found that vehicle-treated animals had significantly fewer mature oligodendrocytes (Figure 3H, 3I, and 3L) based on the number of cells

expressing the myelin-associated enzyme CNPase (2',3'-cyclic-nucleotide 3'-phosphodiesterase), and oligodendrocyte progenitor cells (PDGFR α ⁺ cells, Figure 3M, 3N, and 3Q) compared with those in sham rats. Further, animals treated with either nMSC or aMSCy had significantly more mature oligodendrocytes (Figure 3J through 3L) as well as oligodendrocyte progenitor cells (PDGFR α ⁺ cells; Figure 3O through 3Q) compared with vehicle-treated animals. Last, total protein levels of PDGFR α and myelin basic protein were quantified in tissue lysate of the ipsilateral hemisphere from animals 1 week after MCAO (Figure 3S through 3U). In animals treated with aMSCy there was a significant increase in the total amount of PDGFR α (Figure 3S and 3T) and myelin basic protein (Figure 3S and 3U), suggesting that aMSCy treatment not only induces oligodendrocyte differentiation but also causes these cells to become mature, myelinating oligodendrocytes.

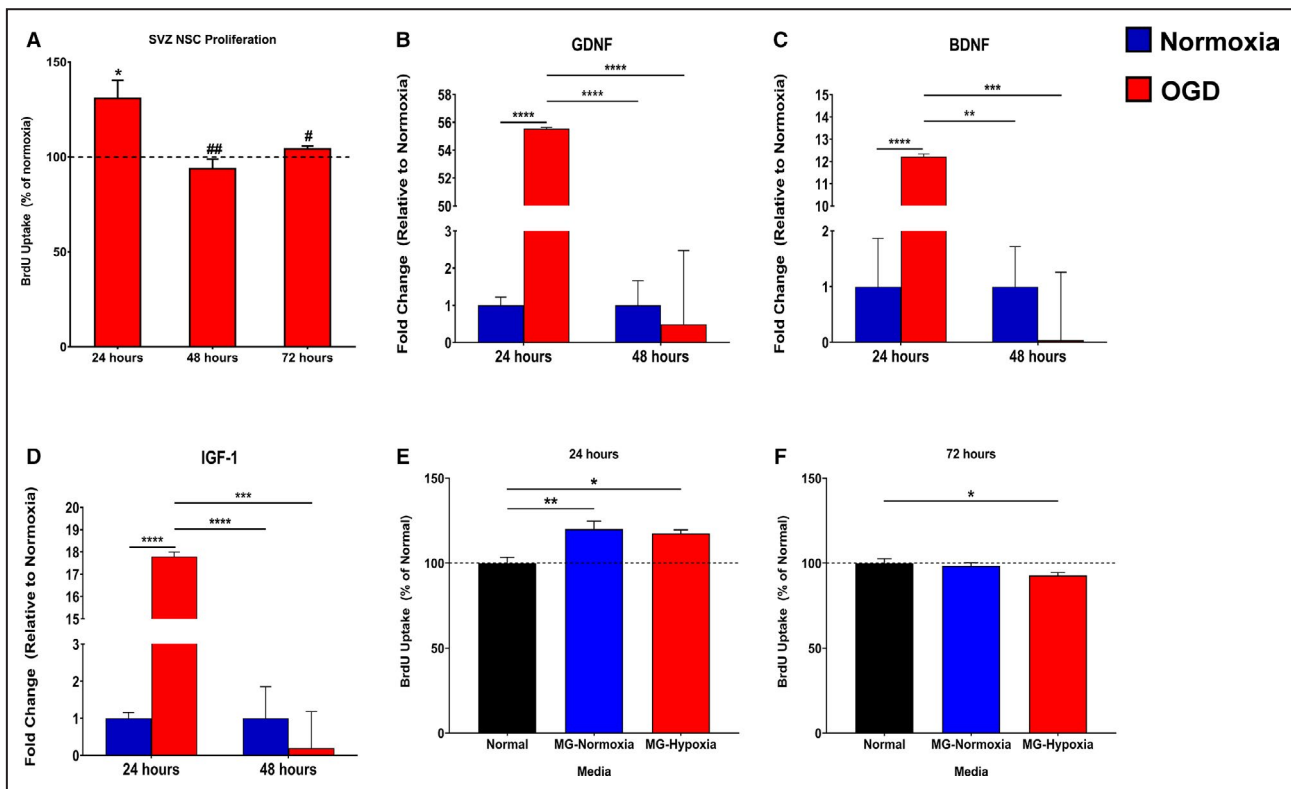


Figure 4. Changes in microglia (MG) and neural stem cells (NSC) after hypoxia.

A, In vitro proliferation of subventricular zone (SVZ)-derived NSC after exposure to oxygen and glucose deprivation (OGD) measured via bromodeoxyuridine (BrdU) uptake and represented as percentage of normoxia. Data are mean \pm SEM; n=5 independent experiments. Normoxia vs OGD data within a given time were compared using a 2-tail unpaired t test. Data across time were compared using nonparametric Kruskal-Wallis 1-way ANOVA. *Compared with normoxia; #Compared with 24 hours OGD. * $P\leq 0.05$, # $P\leq 0.05$, ## $P<0.01$. **B** through **D**, mRNA fold change levels of glia-derived neurotrophic factor (GDNF) (**B**), brain-derived neurotrophic factor (BDNF) (**C**), and insulin-like growth factor (IGF-1) (**D**) from SVZ-derived NSC after exposure to OGD. Data are mean \pm SEM; n=3 independent experiments. Data were analyzed using a 2-way ANOVA with Holm-Sidak multiple-comparison testing. ** $P<0.01$, *** $P<0.001$, **** $P<0.0001$. **E** and **F**, In vitro proliferation of SVZ-derived NSC at 48 hours (**E**) and 72 hours (**F**) after exposure to normal medium (black), conditioned medium from normoxia-primed microglia (blue), or hypoxia-primed microglia (red) measured via BrdU uptake and represented as percentage of normal. Data are mean \pm SEM; n=3 independent experiments. Data were analyzed using a nonparametric Kruskal-Wallis 1-way ANOVA. * $P\leq 0.05$, ** $P<0.01$.

Changes in Microglia and NSC After Hypoxia

To further investigate the effect of reduced oxygen on neural progenitor cells, neurosphere cultures were subjected to *in vitro* OGD. We found that in contrast to the *in vivo* conditions, OGD induced an increase in NPC proliferation, measured via bromodeoxyuridine uptake, 24 hours after exposure to OGD, but this increase was not sustained beyond 24 hours (Figure 4A). Additionally, mRNA levels of glia-derived neurotrophic factor (Figure 4B), brain-derived neurotrophic factor (Figure 4C), and IGF-1 (insulin-like growth factor 1; Figure 4D) were all significantly increased in neurosphere extracts 24 hours after OGD, but by 48 hours these mRNA levels were significantly decreased to almost nonexistent levels. To determine whether a change in neurotrophic factor production results from a change in cell number or viability of the culture, we counted the number of NPC at different time points after OGD and performed MTT, LDH, and terminal deoxynucleotidyl transferase dUTP nick end labeling. We observed that the number of NPC was not significantly changed 48 hours after OGD, although the viability of the culture was reduced (Figure S5). No sign of toxicity or apoptosis was observed in culture following OGD (Figures S5 and S6). Thus, increased production of neurotrophic factors 24 hours following OGD is not simply due to an increased number of cells in culture. We next asked whether the effect on NPC proliferation *in vivo* reflects a combined effect of OGD and microglia. Previous studies have implicated TNF- α secreted by activated microglia as an inhibitor of NPC function.^{8,9} To address this, neurospheres were grown in normal medium, conditioned medium from normoxia-primed microglia, and conditioned medium from OGD-primed microglia, and proliferation was measured via bromodeoxyuridine uptake. We found that when grown in medium from OGD-primed microglia, NPC had a small but significantly reduced proliferation compared with NPC grown in normal medium or medium from normoxia-primed microglia at both 48 hours (Figure 4E) and 72 hours (Figure 4F). This agrees with our result that secreted levels of IL-6 and TNF- α were significantly increased 48 hours after OGD compared with levels at 24 hours (Figure 2O and 2P, respectively).

MSC Promote NSC Function and Differentiation

To further investigate the effect of MSC on NPC phenotype, we examined the effect of MSC on trophic factor production level in OGD conditions. As shown earlier, NSC demonstrate trophic factor loss following OGD; however, IFN- γ activation causes significant increases in MSC production of glia-derived neurotrophic factor and IGF-1 (Figure S7, Table S1), suggesting that

MSC might aid in sustaining trophic factor levels after OGD. We found that, after OGD-priming, NPC grown in a coculture system with aMSCy have significantly increased production of mRNA for glia-derived neurotrophic factor (Figure 5A), brain-derived neurotrophic factor (Figure 5B), and IGF-1 (Figure 5C) after both 24 and 48 hours.

Normally, NSC grow as neurospheres in suspension (Figure 5D). However, after culture in conditioned medium from either nMSC or aMSCy, these cells adhere to the plate and put out fine processes (Figure 5E and 5F), similar to their morphology while undergoing differentiation. To determine how MSC-conditioned medium affected the NPC cell cycle, bromodeoxyuridine flow cytometry was performed to determine the percentage of cells in each of the cell cycle stages (Figure 5G through 5L). We found that when grown in nMSC-conditioned medium and, to a larger extent, aMSCy-conditioned medium, NPC had significantly fewer cells in the S phase of the cell cycle and significantly more cells in the G0/1 phase of the cell cycle at 24 hours (Figure 5J), 48 hours (Figure 5K), and 72 hours (Figure 5L), suggesting that these cells are no longer proliferating and are exiting the cell cycle—a process that occurs when these cells undergo differentiation.

To determine what types of cells these NPC were becoming, they were grown for 6 days in either normal medium, nMSC-conditioned medium, or aMSCy-conditioned medium, at which point lineage-specific markers were analyzed by Western blot (Figure 5M through 5R, Table S2). We found that, when the cells were grown in nMSC-conditioned medium and, to a significant extent, aMSCy-conditioned medium, there was reduced expression of the astrocyte marker glial fibrillary acidic protein (Figure 5N), the neuron marker neurofilament L (Figure 5Q), and the stem-cell marker Sox2 (Figure 5R), with significantly increased expression of the oligodendrocyte lineage marker PDGFR α (Figure 5O). Together, these data support our *in vivo* observations and demonstrate that conditioned medium from MSC, with a larger effect from aMSCy, causes NPC to differentiate toward an oligodendrocyte lineage.

Identification of the MSC Secretome

The protein secretome from MSC (for MSC identification and characterization see Figures S8 and S9) has been described under various conditions⁶⁷⁻⁷¹; however, it is unknown what factors secreted by MSC induce NPC oligodendrogenesis and phenotype change in microglia subjected to hypoxic conditions. In addition, the differences in secreted proteins between nMSC and aMSCy have never been described before. Based on the data presented in this study, aMSCy exert a more potent effect on microglial phenotype and induce

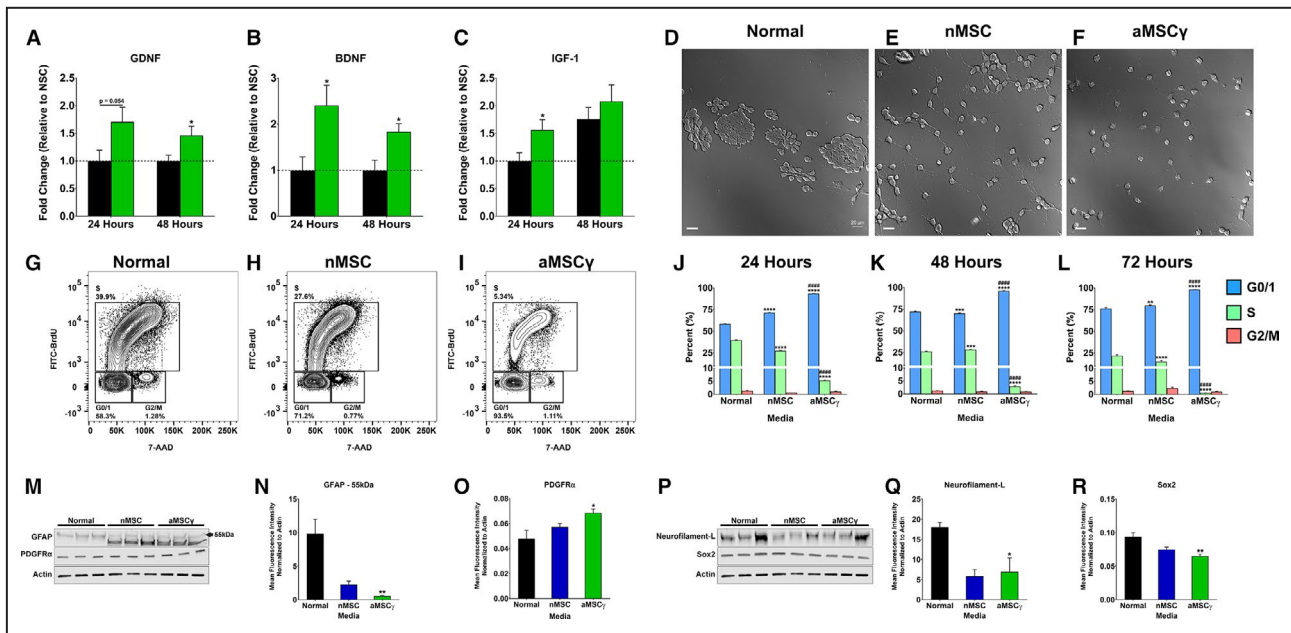


Figure 5. Mesenchymal stem cells (MSC) promote neural stem-cell (NSC) function and differentiation.

A through **C**, mRNA fold change levels of glia-derived neurotrophic factor (GDNF) (**A**), brain-derived neurotrophic factor (BDNF) (**B**), and insulin-like growth factor 1 (IGF-1) (**C**) from oxygen and glucose deprivation (OGD)-primed subventricular zone (SVZ)-derived NSC after coculture with aMSCy in a ratio of aMSCy:NSC of 1:10. Data are mean±SEM; n=3 independent experiments. Data were analyzed using a 2-way ANOVA with Holm-Sidak multiple comparison testing. * $P < 0.05$. **D** through **F**, DIC imaging of NSC grown in normal medium (**D**), nMSC-conditioned medium (**E**), or aMSCy-conditioned medium (**F**). Scale bar represents 20 μm . **G** through **I**, Concatenated contour plots from bromodeoxyuridine (BrdU) flow cytometry of NSC grown in normal medium (**G**), nMSC-conditioned medium (**H**), or aMSCy-conditioned medium (**I**). **J** through **L**, Quantification of cell cycle stages G0/1 (blue), S (green), and G2/M (pink) from BrdU flow cytometry of NSC grown in normal medium, nMSC-conditioned medium, or aMSCy-conditioned medium at 24 hours (**J**), 48 hours (**K**), and 72 hours (**L**). Data are mean±SEM; n=3 independent experiments. Data were analyzed using 2-way ANOVA with Holm-Sidak multiple comparison testing. *Compared with Normal. #Compared with nMSC. ** $P < 0.01$, *** $P < 0.001$, **** $P < 0.0001$, ##### $P < 0.00001$. **M** through **O**, Western blots of lineage-specific markers GFAP (glial fibrillary acidic protein) (astrocytes) and platelet-derived growth factor receptor α (PDGFR α) (oligodendrocytes) (**M**) and their quantification (**N** and **O**) from NSC grown in normal medium, nMSC-conditioned medium, or aMSCy-conditioned medium for 6 days normalized to actin. **P** through **R**, Western blots of lineage-specific markers neurofilament L (neurons) and Sox2 (stem cells) (**P**) and their quantification (**Q** and **R**) from NSC grown in normal medium, nMSC-conditioned medium, or aMSCy-conditioned medium for 6 days normalized to actin. Data are mean±SEM; n=3 independent experiments. Data were analyzed using nonparametric Kruskal-Wallis 1-way ANOVA. *Compared with Normal. * $P < 0.05$, ** $P < 0.01$. 7-AAD indicates 7-aminoactinomycin D; aMSCy, interferon- γ -activated mesenchymal stem cells; DIC, differential interference contrast; and nMSC, naive mesenchymal stem cells.

oligodendrogenesis and myelination. Therefore, in order to determine what potential protein factors secreted by the aMSCy were responsible for the changes we observed in vitro and in vivo, proteomics analyses of the MSC and aMSCy secretome were performed via mass spectrometry (Figure 6; for the full list of proteins see Tables S3 and S4). From this approach, 244 proteins were identified, with 16 proteins being unique to nMSC, 27 proteins being unique to aMSCy, and the remaining 201 proteins being secreted by both MSC types (Figure 6A). Additionally, secreted proteins belong to many different biologic processes and protein classes with almost a quarter of proteins (21.6%) belonging to the signaling molecule or extracellular matrix classes (Figure 6B). Further, the secretome between both experimental and biological replicates remains consistent with very little variability between replicates

both in the number of secreted proteins and the amount of those proteins (Figure 6C). Furthermore, with ex vivo IFN- γ activation, there are 18 proteins that are significantly upregulated (>2-fold increase, $P < 0.008$) and 21 proteins that are significantly downregulated (>2-fold decrease, $P < 0.008$) compared with nMSC (Figure 6D). Notably, aMSCy but not nMSC induce upregulation of CSPG4 (chondroitin sulfate proteoglycan 4), an important extracellular signal and a hallmark protein of oligodendrocyte precursor cells (OPC).⁷² In addition, we observed upregulation of BMP1 (bone morphogenetic protein 1), which promotes the generation of mature myelinating oligodendrocytes in vivo.⁷³ MetaCore (Thomson Reuters, Toronto, Ontario, Canada) pathway analysis of these differential proteins resulted in 24 significantly enriched pathways (Tables S3 and S4, false discovery rate, $FDR < 0.05$).

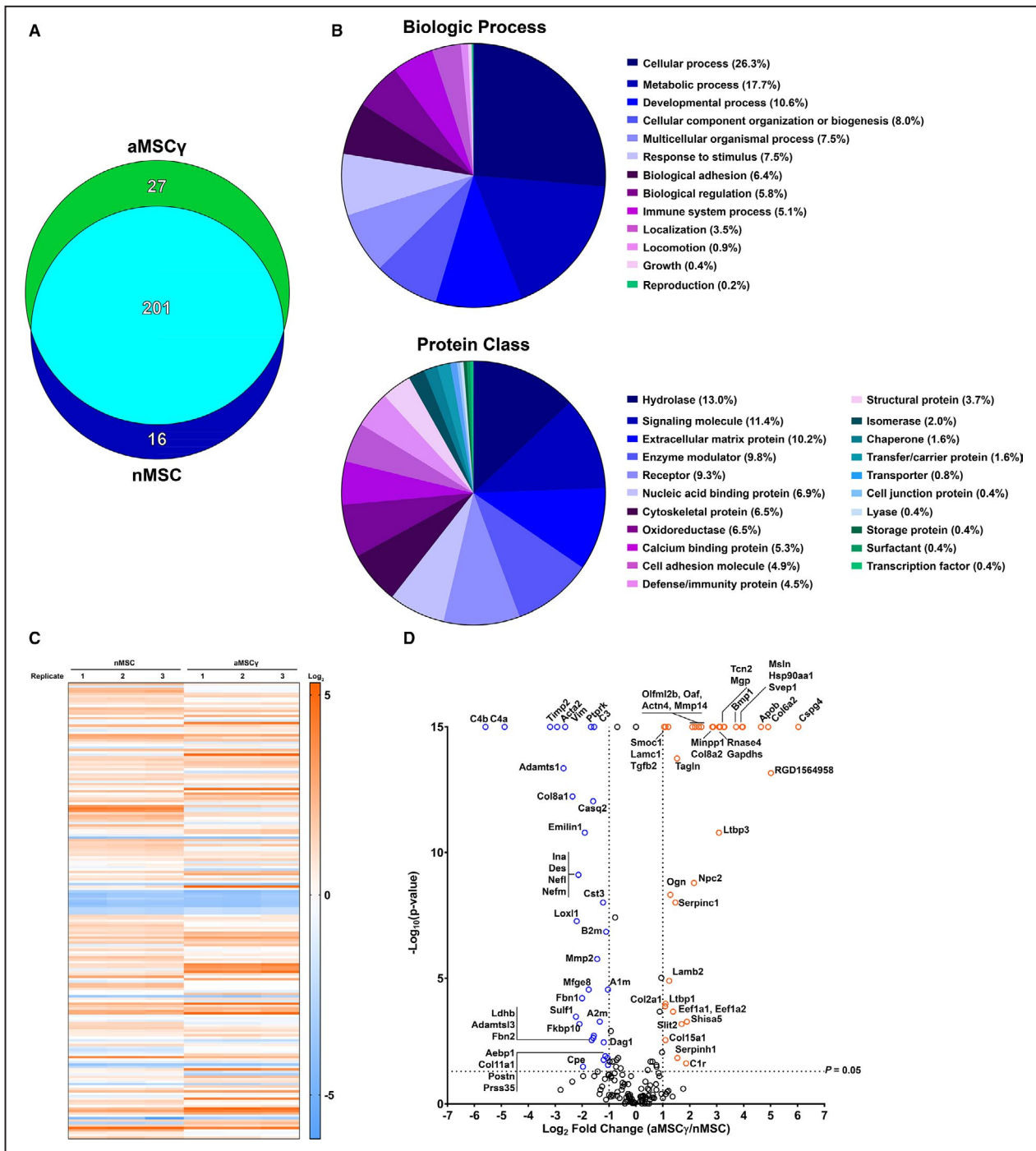


Figure 6. Identification of the interferon- γ -activated and naive mesenchymal stem cell (aMSCy, nMSC) secretome. **A**, Venn diagram illustrating the number of proteins identified in each medium type. **B**, Biologic process (top chart) and protein class (bottom chart) breakdowns of identified proteins. **C**, Heat map analysis of biological replicates from both nMSC- and aMSCy-conditioned media. **D**, Volcano plot showing differentially secreted proteins between aMSCy and nMSC. Positive fold changes indicate higher expression in aMSCy, and negative fold changes indicate higher expression in nMSC. Data are mean \pm SEM; n=3 independent experiments. Data were analyzed by a permutation test with unadjusted significance level $P < 0.05$ corrected by the Benjamini-Hochberg procedure (new $P < 0.008$).

DISCUSSION

This study reports several important observations. We first showed that, when administered 3 hours

after ischemic injury, MSC treatment leads to a significant functional recovery of treated animals as a direct result of preservation of brain parenchyma. In that regard, for various reasons, including delay to

treatment and lack of recognition of stroke symptoms, no stroke therapy can be developed to completely regenerate infarcted tissue or to prevent the formation of an infarct core. Consequently, therapies aimed at limiting the size of the infarct and infarct penumbra are most clinically relevant. Related to this, preservation of the support structure within the penumbra is crucial for long-term functional recovery after stroke. Thus, the observation that MSC treatment as administered in this study can minimize the infarct and penumbra is highly significant. The feasibility of this treatment is similar to that of tissue plasminogen activator, the only treatment currently available for acute ischemic stroke¹⁶ within 3 hours of onset. Because MSC do not induce a host immune response, they could be banked as a blood-bank product and should be available for treatment on thawing.

Second, we demonstrated that MSC reverse the proinflammatory phenotype of microglia induced by hypoxia and ischemia. Additionally, treatment of stroke animals by both nMSC and aMSCy leads to a significant reduction in CD68⁺ monocytes and microglia, which may contribute to the preservation of brain tissue and the reduction in infarct size. This observation suggests that MSC are effective modifiers of microglial or monocyte phenotype, and their effect may be applicable to other brain insults characterized by increased inflammation. It should be noted that Iba-1 and CD68 recognize both microglia and infiltrating monocytes, which can present a different phenotype. Thus, we cannot exclude the possibility that the detected effect reflects both cell types.

Third, we showed that aMSCy are more potent than nMSC. Although both nMSC and aMSCy lead to equivalent levels of functional recovery, aMSCy exert 2 main molecular and cellular advantages that we believe make them a better therapeutic option. We showed (1) that, compared with nMSC, aMSCy cause significant increases in anti-inflammatory cytokine secretion by microglia with corresponding decreases in proinflammatory cytokines, and (2) that treatment with aMSCy in vivo more effectively induces oligodendrocyte differentiation and myelination. Thus, we propose that aMSCy would be a significantly more effective therapeutic agent than nMSC.

Fourth, in contrast to previous reports, we observed that ischemia suppresses the proliferation of neural progenitor cells in the SVZ and that neurogenesis is not induced either by ischemia or by MSC treatment. Therefore, future therapeutic avenues should test the regenerative efficacy of aMSCy in combination with proneurogenic approaches.

Fifth, we showed that treatment with aMSCy after stroke induced a significant increase in the number of oligodendrocyte progenitor cells (OPC)

in the SVZ, ultimately leading to their differentiation and increased myelin production. We also demonstrated a significant increase in the number of OPC and mature oligodendrocytes in the striatum of stroke animals treated with aMSCy. To start to address the mechanism underlying aMSCy-induced oligodendrogenesis, we compared the secretome of aMSCy and nMSC. We unraveled a set of proteins that may be involved in the differential effect exerted by aMSCy, which may underlie the robust pro-oligodendrogenic response seen with aMSCy treatment. For example, we observed upregulation of BMP1, which promotes the generation of mature myelinating oligodendrocytes in vivo.⁷³ Further, we observed upregulation of chondroitin sulfate proteoglycan 4 (CSPG4, also known as neuron-glia antigen 2), an important extracellular signal and a hallmark protein of the OPC. Mutations in CSPG4 cause OPC dysfunction and are implicated in familial schizophrenia.⁷⁴ Interestingly, CSPG4 is highly expressed by brain pericytes, an important component of the neurovascular unit. Thus, it is possible that aMSCy affect the composition of the blood-brain barrier.⁷⁵ This may have implications for the integrity of the blood-brain barrier and for brain function.⁷⁶ In support of this notion, the administration of MSC-derived extracellular vesicles following spinal cord injury enhanced the integrity of the blood–spinal cord barrier by affecting pericyte signaling.⁷⁷ Another important extracellular component upregulated in aMSCy is collagen α -2(VI), 1 of the 3 α -chains of type VI collagen, a protein known to have a protective effect in the central nervous system under stress conditions, including enhancement of neural cell viability and reduction of oxidative stress.⁷⁸ Importantly, an earlier study suggested that collagen VI regulates proper myelination in the peripheral nervous system.⁷⁹ Interestingly, we observed that Svp1 (sushi, von Willebrand factor type A, EGF, and pentraxin domain containing 1) and SRPX2 (sushi repeat containing protein X-linked 2) are differentially upregulated in the aMSCy. SRPX2 is implicated in angiogenesis and is a ligand of the urokinase plasminogen activator surface receptor.⁸⁰ In addition, it was shown to promote synapse formation.⁸¹ On the other hand, we observed downregulation of the immunomodulator SEMA7A (Semaphorin 7A) involved in inflammatory responses. SEMA7A is also known as the John-Milton-Hagen blood group antigen, an 80-kDa glycoprotein expressed on activated lymphocytes and erythrocytes. Interestingly, SEMA5A is an inhibitor of axonal growth expressed by oligodendrocytes and their precursor cells in the developing optic nerve and is thought to contribute to the inhibition of CNS axon growth by oligodendrocyte lineage cells after injury.⁸² In addition, we observed downregulation of

olm13- expressed on microglia.⁸³ Of note, Q6AYQ9 peptidyl-prolyl *cis-trans* isomerase is expressed in MSC, but its role and the significance of its levels are yet to be understood.

One limitation of this study is the small sample size. A prerequisite for the successful translation of this approach would be the examination of this treatment in a large cohort. In addition, further studies are warranted in order to determine whether post-stroke treatment with aMSCy promotes neuronal replacement. In that regard the efficacy of a combined therapy of aMSCy with other stem cell-based promising treatments that promote neuronal production is an avenue worth exploring. For example, vasculoprotective drugs, such as activated protein C, a serine protease known to promote cytoprotective signaling in the ischemic brain endothelium at the blood-brain barrier,⁸⁴ have been shown to stimulate neuronal production by transplanted human NSC, promote circuit restoration, and improve functional recovery.⁸⁵

In summary, our study reveals important information that advances our understanding of the efficacy and therapeutic potential of MSC for the treatment of ischemic stroke. It provides a potent alternative in the form of aMSCy and unravels its mechanism of action, which may facilitate drug development.

ARTICLE INFORMATION

Received June 11, 2019; accepted February 17, 2020.

Affiliations

From the Departments of Anatomy and Cell Biology (M.K.T., T.K.L.S., K.L.L., O.L.), Chemistry (M.R.P., S.M.C.), and Surgery (A.M.B.), University of Illinois at Chicago, IL.

Acknowledgments

The authors would like to thank Dr Weiguo Li, the director of the Preclinical Imaging Core in the University of Illinois at Chicago Research Resources Center and his graduate student, Jin Gao, for their help with the MRI studies and the University of Illinois at Chicago Core for Research Bioinformatics for their help with analysis of mass spectrometry data. The authors would also like to thank Dr Ernesto Bongarzone for generously providing us with the CNPase antibody.

Author contributions: Tobin designed the research studies, conducted experiments, acquired and analyzed data, and wrote the manuscript. Lopez conducted experiments and analyzed data. Pergande designed the research studies, conducted experiments, acquired and analyzed data, and wrote the manuscript. Stephen wrote the manuscript. Cologna designed the research studies, conducted experiments, and acquired and analyzed data. Bartholomew designed the research studies and analyzed data. Lazarov designed the research studies and wrote the manuscript. All authors critically revised and approved the manuscript.

Sources of Funding

This work was supported by National Institute on Aging R01-AG033570, R01-AG060238, R01-AG062251, R21-AG061628, University of Illinois at Chicago, Center for Clinical and Translational Science CCTS-0512-06 (Lazarov); National Heart, Lung, and Blood Institute/T32-HL007692, and American Heart Association AHA/15PRE25080088 (Tobin); University of Illinois at Chicago Abraham Lincoln Fellowship (Pergande); National Institute of Allergy and Infectious Diseases/P01-AI089556 (Bartholomew); University of Illinois at Chicago Department of Chemistry Startup Funds, Ara Parseghian Medical Research Fund (Cologna).

Disclosures

None.

Supplementary Materials

Video S1

Data S1

Tables S1–S4

Figures S1–S9

Reference 60

REFERENCES

- Donnan GA, Fisher M, Macleod M, Davis SM. Stroke. *Lancet*. 2008;371:1612–1623.
- Go AS, Mozaffarian D, Roger VL, Benjamin EJ, Berry JD, Blaha MJ, Dai S, Ford ES, Fox CS, Franco S, et al. American Heart Association Statistics Committee and Stroke Statistics Subcommittee. Heart disease and stroke statistics—2014 update: a report from the American Heart Association. *Circulation*. 2014;129:e28–e292.
- Benjamin EJ, Blaha MJ, Chiuve SE, Cushman M, Das SR, Deo R, de Ferranti SD, Floyd J, Fornage M, Gillespie C, et al. American Heart Association Statistics Committee and Stroke Statistics Subcommittee. Heart disease and stroke statistics—2017 update: a report from the American Heart Association. *Circulation*. 2017;135:e146–e603.
- Towfighi A, Saver JL. Stroke declines from third to fourth leading cause of death in the United States: historical perspective and challenges ahead. *Stroke*. 2011;42:2351–2355.
- Schwamm LH, Ali SF, Reeves MJ, Smith EE, Saver JL, Messe S, Bhatt DL, Grau-Sepulveda MV, Peterson ED, Fonarow GC. Temporal trends in patient characteristics and treatment with intravenous thrombolysis among acute ischemic stroke patients at Get With The Guidelines-Stroke hospitals. *Circ Cardiovasc Qual Outcomes*. 2013;6:543–549.
- Nogueira RG, Jadhav AP, Haussen DC, Bonafe A, Budzik RF, Bhuva P, Yavagal DR, Ribo M, Cognard C, Hanel RA, et al. DAWN Trial Investigators. Thrombectomy 6 to 24 hours after stroke with a mismatch between deficit and infarct. *N Engl J Med*. 2018;378:11–21.
- Albers GW, Marks MP, Kemp S, Christensen S, Tsai JP, Ortega-Gutierrez S, McTaggart RA, Torbey MT, Kim-Tenser M, Leslie-Mazwi T, et al. DEFUSE 3 Investigators. Thrombectomy for stroke at 6 to 16 hours with selection by perfusion imaging. *N Engl J Med*. 2018;378:708–718.
- Iosif RE, Ahlenius H, Ekdahl CT, Darsalia V, Thored P, Jovinge S, Kokaia Z, Lindvall O. Suppression of stroke-induced progenitor proliferation in adult subventricular zone by tumor necrosis factor receptor 1. *J Cereb Blood Flow Metab*. 2008;28:1574–1587.
- Iosif RE, Ekdahl CT, Ahlenius H, Pronk CJ, Bonde S, Kokaia Z, Jacobsen SE, Lindvall O. Tumor necrosis factor receptor 1 is a negative regulator of progenitor proliferation in adult hippocampal neurogenesis. *J Neurosci*. 2006;26:9703–9712.
- Ziv Y, Ron N, Butovsky O, Landa G, Sudai E, Greenberg N, Cohen H, Kipnis J, Schwartz M. Immune cells contribute to the maintenance of neurogenesis and spatial learning abilities in adulthood. *Nat Neurosci*. 2006;9:268–275.
- Ziv Y, Avidan H, Pluchino S, Martino G, Schwartz M. Synergy between immune cells and adult neural stem/progenitor cells promotes functional recovery from spinal cord injury. *Proc Natl Acad Sci USA*. 2006;103:13174–13179.
- Jakubs K, Bonde S, Iosif RE, Ekdahl CT, Kokaia Z, Kokaia M, Lindvall O. Inflammation regulates functional integration of neurons born in adult brain. *J Neurosci*. 2008;28:12477–12488.
- Schilling M, Besselmann M, Muller M, Strecker JK, Ringelstein EB, Kiefer R. Predominant phagocytic activity of resident microglia over hematogenous macrophages following transient focal cerebral ischemia: an investigation using green fluorescent protein transgenic bone marrow chimeric mice. *Exp Neurol*. 2005;196:290–297.
- Denes A, Vidyasagar R, Feng J, Narvainen J, McColl BW, Kauppinen RA, Allan SM. Proliferating resident microglia after focal cerebral ischaemia in mice. *J Cereb Blood Flow Metab*. 2007;27:1941–1953.
- Thored P, Heldmann U, Gomes-Leal W, Gisler R, Darsalia V, Taneera J, Nygren JM, Jacobsen SE, Ekdahl CT, Kokaia Z, et al. Long-term accumulation of microglia with proneurogenic phenotype concomitant with persistent neurogenesis in adult subventricular zone after stroke. *Glia*. 2009;57:835–849.

16. Tobin MK, Bonds JA, Minshall RD, Pelligrino DA, Testai FD, Lazarov O. Neurogenesis and inflammation after ischemic stroke: what is known and where we go from here. *J Cereb Blood Flow Metab.* 2014;34:1573–1584.
17. Liu J, Solway K, Messing RO, Sharp FR. Increased neurogenesis in the dentate gyrus after transient global ischemia in gerbils. *J Neurosci.* 1998;18:7768–7778.
18. Arvidsson A, Collin T, Kirik D, Kokaia Z, Lindvall O. Neuronal replacement from endogenous precursors in the adult brain after stroke. *Nat Med.* 2002;8:963–970.
19. Lichtenwalner RJ, Parent JM. Adult neurogenesis and the ischemic forebrain. *J Cereb Blood Flow Metab.* 2006;26:1–20.
20. Tsai YW, Yang YR, Wang PS, Wang RY. Intermittent hypoxia after transient focal ischemia induces hippocampal neurogenesis and c-Fos expression and reverses spatial memory deficits in rats. *PLoS One.* 2011;6:e24001.
21. Tonchev AB. Brain ischemia, neurogenesis, and neurotrophic receptor expression in primates. *Arch Ital Biol.* 2011;149:225–231.
22. Tonchev AB, Yamashita T, Zhao L, Okano HJ, Okano H. Proliferation of neural and neuronal progenitors after global brain ischemia in young adult macaque monkeys. *Mol Cell Neurosci.* 2003;23:292–301.
23. Ohab JJ, Fleming S, Blesch A, Carmichael ST. A neurovascular niche for neurogenesis after stroke. *J Neurosci.* 2006;26:13007–13016.
24. Parent JM, Vexler ZS, Gong C, Derugin N, Ferrero DM. Rat forebrain neurogenesis and striatal neuron replacement after focal stroke. *Ann Neurol.* 2002;52:802–813.
25. Zhang ZG, Chopp M. Neurorestorative therapies for stroke: underlying mechanisms and translation to the clinic. *Lancet Neurol.* 2009;8:491–500.
26. Liu X, Xia J, Wang L, Song Y, Yang J, Yan Y, Ren H, Zhao G. Efficacy and safety of ginsenoside-Rd for acute ischaemic stroke: a randomized, double-blind, placebo-controlled, phase II multicenter trial. *Eur J Neurol.* 2009;16:569–575.
27. Zhao S, Wehner R, Bornhauser M, Wassmuth R, Bachmann M, Schmitz M. Immunomodulatory properties of mesenchymal stromal cells and their therapeutic consequences for immune-mediated disorders. *Stem Cells Dev.* 2010;19:607–614.
28. Liu Y, Wang L, Kikuri T, Akiyama K, Chen C, Xu X, Yang R, Chen W, Wang S, Shi S. Mesenchymal stem cell-based tissue regeneration is governed by recipient T lymphocytes via IFN- γ and TNF- α . *Nat Med.* 2011;17:1594–1601.
29. Castillo-Melendez M, Yawno T, Jenkin G, Miller SL. Stem cell therapy to protect and repair the developing brain: a review of mechanisms of action of cord blood and amnion epithelial derived cells. *Front Neurosci.* 2013;7:194.
30. Moradi F, Haji Ghasem Kashani M, Ghorbanian MT, Lashkarbolouki T. Spontaneous expression of neurotrophic factors and TH, Nurr1, Nestin genes in long-term culture of bone marrow mesenchymal stem cells. *Cell J.* 2012;13:243–250.
31. Sadan O, Melamed E, Offen D. Intrastriatal transplantation of neurotrophic factor-secreting human mesenchymal stem cells improves motor function and extends survival in R6/2 transgenic mouse model for Huntington's disease. *PLoS Curr.* 2012;4:e4f7f6dc013d014e.
32. Sadan O, Shemesh N, Barzilay R, Dadon-Nahum M, Blumenfeld-Katzir T, Assaf Y, Yeshurun M, Djaldetti R, Cohen Y, Melamed E, et al. Mesenchymal stem cells induced to secrete neurotrophic factors attenuate quinolinic acid toxicity: a potential therapy for Huntington's disease. *Exp Neurol.* 2012;234:417–427.
33. Chen JR, Cheng GY, Sheu CC, Tseng GF, Wang TJ, Huang YS. Transplanted bone marrow stromal cells migrate, differentiate and improve motor function in rats with experimentally induced cerebral stroke. *J Anat.* 2008;213:249–258.
34. Li Y, Chen J, Chen XG, Wang L, Gautam SC, Xu YX, Katakowski M, Zhang LJ, Lu M, Janakiraman N, et al. Human marrow stromal cell therapy for stroke in rat: neurotrophins and functional recovery. *Neurology.* 2002;59:514–523.
35. Nomura T, Honmou O, Harada K, Houkin K, Hamada H, Kocsis JD. IV infusion of brain-derived neurotrophic factor gene-modified human mesenchymal stem cells protects against injury in a cerebral ischemia model in adult rat. *Neuroscience.* 2005;136:161–169.
36. Honma T, Honmou O, Iihoshi S, Harada K, Houkin K, Hamada H, Kocsis JD. Intravenous infusion of immortalized human mesenchymal stem cells protects against injury in a cerebral ischemia model in adult rat. *Exp Neurol.* 2006;199:56–66.
37. Koh SH, Kim KS, Choi MR, Jung KH, Park KS, Chai YG, Roh W, Hwang SJ, Ko HJ, Huh YM, Kim HT, et al. Implantation of human umbilical cord-derived mesenchymal stem cells as a neuroprotective therapy for ischemic stroke in rats. *Brain Res.* 2008;1229:233–248.
38. Lim JY, Jeong CH, Jun JA, Kim SM, Ryu CH, Hou Y, Oh W, Chang JW, Jeun SS. Therapeutic effects of human umbilical cord blood-derived mesenchymal stem cells after intrathecal administration by lumbar puncture in a rat model of cerebral ischemia. *Stem Cell Res Ther.* 2011;2:38.
39. Gutierrez-Fernandez M, Rodriguez-Frutos B, Ramos-Cejudo J, Otero-Ortega L, Fuentes B, Vallejo-Cremades MT, Sanz-Cuesta BE, Diez-Tejedor E. Comparison between xenogeneic and allogeneic adipose mesenchymal stem cells in the treatment of acute cerebral infarct: proof of concept in rats. *J Transl Med.* 2015;13:46.
40. Liu N, Zhang Y, Fan L, Yuan M, Du H, Cheng R, Liu D, Lin F. Effects of transplantation with bone marrow-derived mesenchymal stem cells modified by survivin on experimental stroke in rats. *J Transl Med.* 2011;9:105.
41. Lowrance SA, Fink KD, Crane A, Matyas J, Dey ND, Matchynski JJ, Thibo T, Reinke T, Kippe J, Hoffman C, et al. Bone-marrow-derived mesenchymal stem cells attenuate cognitive deficits in an endothelin-1 rat model of stroke. *Restor Neurol Neurosci.* 2015;33:579–588.
42. Quittet MS, Touzani O, Sindji L, Cayon J, Fillesoy F, Toutain J, Divoux D, Marteau L, Lecocq M, Roussel S, et al. Effects of mesenchymal stem cell therapy, in association with pharmacologically active microcarriers releasing VEGF, in an ischaemic stroke model in the rat. *Acta Biomater.* 2015;15:77–88.
43. Toyoshima A, Yasuhara T, Kameda M, Morimoto J, Takeuchi H, Wang F, Sasaki T, Sasada S, Shinko A, Wakamori T, et al. Intra-arterial transplantation of allogeneic mesenchymal stem cells mounts neuroprotective effects in a transient ischemic stroke model in rats: analyses of therapeutic time window and its mechanisms. *PLoS One.* 2015;10:e0127302.
44. Wei L, Fraser JL, Lu ZY, Hu X, Yu SP. Transplantation of hypoxia preconditioned bone marrow mesenchymal stem cells enhances angiogenesis and neurogenesis after cerebral ischemia in rats. *Neurobiol Dis.* 2012;46:635–645.
45. Xin H, Li Y, Liu Z, Wang X, Shang X, Cui Y, Zhang ZG, Chopp M. MiR-133b promotes neural plasticity and functional recovery after treatment of stroke with multipotent mesenchymal stromal cells in rats via transfer of exosome-enriched extracellular particles. *Stem Cells.* 2013;31:2737–2746.
46. Yamauchi T, Kuroda Y, Morita T, Shichinohe H, Houkin K, Dezawa M, Kuroda S. Therapeutic effects of human multilineage-differentiating stress enduring (MUSE) cell transplantation into infarct brain of mice. *PLoS One.* 2015;10:e0116009.
47. Yang C, Liu H, Liu D. Mutant hypoxia-inducible factor 1 α modified bone marrow mesenchymal stem cells ameliorate cerebral ischemia. *Int J Mol Med.* 2014;34:1622–1628.
48. Moniche F, Gonzalez A, Gonzalez-Marcos JR, Carmona M, Pinero P, Espigado I, Garcia-Solis D, Cayuela A, Montaner J, Boada C, et al. Intra-arterial bone marrow mononuclear cells in ischemic stroke: a pilot clinical trial. *Stroke.* 2012;43:2242–2244.
49. Diez-Tejedor E, Gutierrez-Fernandez M, Martinez-Sanchez P, Rodriguez-Frutos B, Ruiz-Ares G, Lara ML, Gimeno BF. Reparative therapy for acute ischemic stroke with allogeneic mesenchymal stem cells from adipose tissue: a safety assessment: a phase II randomized, double-blind, placebo-controlled, single-center, pilot clinical trial. *J Stroke Cerebrovasc Dis.* 2014;23:2694–2700.
50. Moniche F, Rosado-de-Castro PH, Escudero I, Zapata E, de la Torre Laviana FJ, Mendez-Otero R, Carmona M, Pinero P, Bustamante A, Lebrato L, et al. Increasing dose of autologous bone marrow mononuclear cells transplantation is related to stroke outcome: results from a pooled analysis of two clinical trials. *Stem Cells Int.* 2016;2016:8657173.
51. Suarez-Monteagudo C, Hernandez-Ramirez P, Alvarez-Gonzalez L, Garcia-Maeso I, de la Cuetara-Bernal K, Castillo-Diaz L, Bringas-Vega ML, Martinez-Aching G, Morales-Chacon LM, Baez-Martin MM, et al. Autologous bone marrow stem cell neurotransplantation in stroke patients. An open study. *Restor Neurol Neurosci.* 2009;27:151–161.
52. Battistella V, de Freitas GR, da Fonseca LM, Mercante D, Gutfilen B, Goldenberg RC, Dias JV, Kasai-Brunswick TH, Wajnberg E, Rosado-de-Castro PH, et al. Safety of autologous bone marrow mononuclear cell transplantation in patients with nonacute ischemic stroke. *Regen Med.* 2011;6:45–52.

53. Bhasin A, Srivastava MV, Kumaran SS, Mohanty S, Bhatia R, Bose S, Gaikwad S, Garg A, Airan B. Autologous mesenchymal stem cells in chronic stroke. *Cerebrovasc Dis Extra*. 2011;1:93–104.
54. Honmou O. [Phase III clinical trial using autologous mesenchymal stem cells for stroke patients]. *Nihon Rinsho*. 2016;74:649–654.
55. Steinberg GK, Kondziolka D, Wechsler LR, Lunsford LD, Coburn ML, Billigen JB, Kim AS, Johnson JN, Bates D, King B, et al. Clinical outcomes of transplanted modified bone marrow-derived mesenchymal stem cells in stroke: a phase 1/2a study. *Stroke*. 2016;47:1817–1824.
56. Polchert D, Sobinsky J, Douglas G, Kidd M, Moadsiri A, Reina E, Genrich K, Mehrotra S, Setty S, Smith B, et al. IFN- γ activation of mesenchymal stem cells for treatment and prevention of graft versus host disease. *Eur J Immunol*. 2008;38:1745–1755.
57. Lee S, Szilagyi E, Chen L, Premanand K, DiPietro LA, Ennis W, Bartholomew AM. Activated mesenchymal stem cells increase wound tensile strength in aged mouse model via macrophages. *J Surg Res*. 2013;181:20–24.
58. Faul F, Erdfelder E, Lang AG, Buchner A. G*Power 3: a flexible statistical power analysis program for the social, behavioral, and biomedical sciences. *Behav Res Methods*. 2007;39:175–191.
59. Belayev L, Alonso OF, Busto R, Zhao W, Ginsberg MD. Middle cerebral artery occlusion in the rat by intraluminal suture. Neurological and pathological evaluation of an improved model. *Stroke*. 1996;27:1616–1622; discussion 1623.
60. Wang Y, Zhang Z, Chow N, Davis TP, Griffin JH, Chopp M, Zlokovic BV. An activated protein C analog with reduced anticoagulant activity extends the therapeutic window of tissue plasminogen activator for ischemic stroke in rodents. *Stroke*. 2012;43:2444–2449.
61. Janardhan V, Qureshi AI. Mechanisms of ischemic brain injury. *Curr Cardiol Rep*. 2004;6:117–123.
62. Kim J, Hematti P. Mesenchymal stem cell-educated macrophages: a novel type of alternatively activated macrophages. *Exp Hematol*. 2009;37:1445–1453.
63. Eglitis MA, Mezey E. Hematopoietic cells differentiate into both microglia and macroglia in the brains of adult mice. *Proc Natl Acad Sci USA*. 1997;94:4080–4085.
64. Ginhoux F, Lim S, Hoeffel G, Low D, Huber T. Origin and differentiation of microglia. *Front Cell Neurosci*. 2013;7:45.
65. Holness CL, Simmons DL. Molecular cloning of CD68, a human macrophage marker related to lysosomal glycoproteins. *Blood*. 1993;81:1607–1613.
66. Rivers LE, Young KM, Rizzi M, Jamen F, Psachoulia K, Wade A, Kessar N, Richardson WD. PDGFRA/NG2 glia generate myelinating oligodendrocytes and piriform projection neurons in adult mice. *Nat Neurosci*. 2008;11:1392–1401.
67. Silva NA, Moreira J, Ribeiro-Samy S, Gomes ED, Tam RY, Shoichet MS, Reis RL, Sousa N, Salgado AJ. Modulation of bone marrow mesenchymal stem cell secretome by ECM-like hydrogels. *Biochimie*. 2013;95:2314–2319.
68. Rocha B, Calamia V, Casas V, Carrascal M, Blanco FJ, Ruiz-Romero C. Secretome analysis of human mesenchymal stem cells undergoing chondrogenic differentiation. *J Proteome Res*. 2014;13:1045–1054.
69. Xiao B, Rao F, Guo ZY, Sun X, Wang YG, Liu SY, Wang AY, Guo QY, Meng HY, Zhao Q, et al. Extracellular matrix from human umbilical cord-derived mesenchymal stem cells as a scaffold for peripheral nerve regeneration. *Neural Regen Res*. 2016;11:1172–1179.
70. Maffioli E, Nonnis S, Angioni R, Santagata F, Cali B, Zanotti L, Negri A, Viola A, Tedeschi G. Proteomic analysis of the secretome of human bone marrow-derived mesenchymal stem cells primed by pro-inflammatory cytokines. *J Proteomics*. 2017;166:115–126.
71. Wang X, Chen G, Huang C, Tu H, Zou J, Yan J. Bone marrow stem cells-derived extracellular matrix is a promising material. *Oncotarget*. 2017;8:98336–98347.
72. Birey F, Kokkosis AG, Aguirre A. Oligodendroglia-lineage cells in brain plasticity, homeostasis and psychiatric disorders. *Curr Opin Neurobiol*. 2017;47:93–103.
73. See J, Mamontov P, Ahn K, Wine-Lee L, Crenshaw EB 3rd, Grinspan JB. BMP signaling mutant mice exhibit glial cell maturation defects. *Mol Cell Neurosci*. 2007;35:171–182.
74. de Vrij FM, Bouwkamp CG, Gunhanlar N, Shpak G, Lendemeijer B, Baghdadi M, Gopalakrishna S, Ghazvini M, Li TM, Quadri M, et al. Candidate CSPG4 mutations and induced pluripotent stem cell modeling implicate oligodendrocyte progenitor cell dysfunction in familial schizophrenia. *Mol Psychiatry*. 2019;24:757–771.
75. Sweeney MD, Zhao Z, Montagne A, Nelson AR, Zlokovic BV. Blood-brain barrier: from physiology to disease and back. *Physiol Rev*. 2019;99:21–78.
76. Nation DA, Sweeney MD, Montagne A, Sagare AP, D'Orazio LM, Pachicano M, Sepeshband F, Nelson AR, Buennagel DP, Harrington MG, et al. Blood-brain barrier breakdown is an early biomarker of human cognitive dysfunction. *Nat Med*. 2019;25:270–276.
77. Lu Y, Zhou Y, Zhang R, Wen L, Wu K, Li Y, Yao Y, Duan R, Jia Y. Bone mesenchymal stem cell-derived extracellular vesicles promote recovery following spinal cord injury via improvement of the integrity of the blood-spinal cord barrier. *Front Neurosci*. 2019;13:209.
78. Cescon M, Chen P, Castagnaro S, Gregorio I, Bonaldo P. Lack of collagen VI promotes neurodegeneration by impairing autophagy and inducing apoptosis during aging. *Aging (Albany NY)*. 2016;8:1083–1101.
79. Chen P, Cescon M, Megighian A, Bonaldo P. Collagen VI regulates peripheral nerve myelination and function. *FASEB J*. 2014;28:1145–1156.
80. Eden G, Archinti M, Furlan F, Murphy R, Degryse B. The urokinase receptor interactome. *Curr Pharm Des*. 2011;17:1874–1889.
81. Schirwani S, McConnell V, Willoughby J, Study DDD, Balasubramanian M. Exploring the association between SRPX2 variants and neurodevelopment: how causal is it? *Gene*. 2018;685:50–54.
82. Goldberg JL, Vargas ME, Wang JT, Mandemakers W, Oster SF, Sretavan DW, Barres BA. An oligodendrocyte lineage-specific semaphorin, Sema5A, inhibits axon growth by retinal ganglion cells. *J Neurosci*. 2004;24:4989–4999.
83. Chitnis T, Weiner HL. CNS inflammation and neurodegeneration. *J Clin Invest*. 2017;127:3577–3587.
84. Zlokovic BV, Griffin JH. Cytoprotective protein C pathways and implications for stroke and neurological disorders. *Trends Neurosci*. 2011;34:198–209.
85. Wang Y, Zhao Z, Rege SV, Wang M, Si G, Zhou Y, Wang S, Griffin JH, Goldman SA, Zlokovic BV. 3K3A-activated protein C stimulates post-ischemic neuronal repair by human neural stem cells in mice. *Nat Med*. 2016;22:1050–1055.

SUPPLEMENTAL MATERIAL

DATA S1.

SUPPLEMENTAL METHODS

Chemicals and Reagents

Chemicals and reagents used are listed below with vendors listed in parenthesis. Primers used for qRT-PCR are listed in Table S1 and antibodies are listed in Table S2.

Animals

All animal experiments were approved by the University of Illinois at Chicago Institutional Animal Care and Use Committee. For surgical experiments, female Sprague-Dawley rats (age 14 to 16 weeks, weight 225-275 grams) were purchased from Envigo (Huntingdon, Cambridgeshire, UK) and were group housed and maintained in standard housing conditions (14/10 hour light/dark cycle) with access to food and water *ad libitum*. Post-operatively, animals were singly housed. For neonatal mixed glial cell isolations, breeding pairs of Sprague-Dawley rats (age 8 weeks) were purchased from Charles River Laboratories and were maintained as above. Female breeders were used for up to 3 litters before being replaced as breeders. Animals used for mesenchymal stem cell and subventricular neural stem cell isolation were obtained from an in-house breeding pair.

Middle cerebral artery occlusion

Anesthesia was induced and maintained in isoflurane in 100% oxygen for the duration of the procedure and body temperature was maintained at $37 \pm 0.4^{\circ}\text{C}$ via rectal probe-monitored heating pad. The ventral neck was shaved and remaining hair was removed with depilatory cream. The skin was prepped with 3 alternating wipes of isopropanol wipes and povidone-iodine swabs and an approximately 3.5 cm incision was made. Glandular tissue and fascia was dissected using

a combination of blunt and sharp dissection until the underlying muscles on the right side were visualized. The right omohyoid muscle was resected to expose the common carotid artery (CCA) and the carotid bifurcation. A 0.5 cm section of the proximal common carotid artery was dissected free from surrounding adventitia taking care to not disturb the adjacent vagus nerve. Following CCA dissection, the carotid bifurcation, external carotid artery (ECA), superior thyroid artery, occipital artery, and the internal carotid artery (ICA) were dissected free from surrounding adventitia. The superior thyroid artery and occipital artery were both coagulated and divided to allow for free movement of the ECA. The ECA was then dissected as distally as possible, coagulated, and divided and a loosely tied 5-0 silk suture was tied around the proximal ECA stump. The remaining ICA was dissected distally to expose the bifurcation of the ICA and the pterygopalatine artery. Temporary vessel clips were placed first on the previously dissected 0.5 cm segment of the CCA and then on the ICA as distally as possible. A small arteriotomy was made in the ECA stump and a silicone-coated 4-0 nylon filament (Doccol #404156PK10Re) was inserted through the arteriotomy into the ICA. The 5-0 silk tie was tightened to secure the filament, the ICA vessel clip was removed and the filament was inserted into the ICA until resistance was felt. At this time, the animal received a single BrdU injection (100 mg/kg IP) and the filament was left in place to occlude the middle cerebral artery for 90 minutes. After 90 minutes, the filament was withdrawn, a temporary vessel clip was placed on the ICA, the ECA stump was coagulated to close the arteriotomy, the two vessel clips were removed and the skin was closed. The animal was then placed into a recovery chamber maintained at 30°C and received 2.0 mL of warm saline intraperitoneally. Following a 3-hour recovery period, the animal was re-anesthetized and was administered either vehicle (1X PBS) treatment, 5.0×10^6 nMSC/kg, or 5.0×10^6 aMSC γ /kg intravenously.

Mesenchymal stem cell isolation and culture

Female rats less than 4 weeks of age were euthanized via isoflurane overdose and decapitation. Femurs and tibias were dissected out into ice cold dissection media (50:50 MEM α /F-12, 10% FBS) and washed three times in cold dissection media. The ends of the bones were cut off and bone marrow plugs were flushed out with 10 mL of cold dissection media. Bone marrow plugs were pipetted 10X with a 10 mL serological pipet and were passed through a 70 μ m cell strainer. Using the plunger from a 10 mL syringe, bone marrow plugs were pushed through the cell strainer which was then wash twice with 10 mL ice cold dissection media. The cell suspension was spun at 300g for 10 minutes and the pellets were resuspended in warm growth media (50:50 MEM α /F-12, 10% FBS, 1% antibiotic-antimycotic) and plated at 37°C plus 5% CO₂. After 24 hours, and then every 3 days thereafter, the media was replaced until the cells reached confluency. At that point, cells were trypsinized and underwent magnetic bead purification. Trypsinized cells were counted and 200,000 cells were set aside to use as a “pre-purification” sample. The remaining cells were spun at 300g for 5 minutes and were resuspended in 50 μ L flow buffer (1X DPBS without calcium and magnesium, 2% BSA, 25 mM HEPES, 5 mM EDTA) per 10⁶ cells containing 10 μ g/mL each of biotin anti-rat CD45 and biotin anti-rat CD11b/c (Table S2) and were incubated for 30 minutes at 4°C. Cells were washed with 10X volume of flow buffer and spun at 500g for 10 minutes. The cell pellet was resuspended in 80 μ L flow buffer plus 10 μ L anti-biotin microbeads (Miltenyi Biotec #130-090-485) per 10⁷ cells and incubated for 15 minutes at 4°C. Cells were washed with 10X volume of flow buffer and spun at 500g for 10 minutes. While spinning, an LS column (Miltenyi Biotec #120-000-475) was washed with 3 mL of flow buffer. The cell pellet was resuspended in 3 mL flow buffer and added to the LS column attached to a

QuadroMACS separator (Miltenyi Biotec #130-090-976) and allowed to flow through into a 15 mL conical tube. The column was washed three times with 3 mL flow buffer and collected into the same conical tube, which contains purified mesenchymal stem cells. 5 mL of flow buffer was added to the LS column and the supplied plunger was used to plunge the bound cells (macrophages) into a new 15 mL conical tube. The purified MSCs were counted and 10^5 cells/per tube were taken for phenotype analysis by flow cytometry and the remainder of the cells were put back into culture for continued use. Pre-purification cells, bead-bound macrophages, and purified MSCs were stained and analyzed by flow cytometry to determine the purity of the MSC population. Cells were stained for CD11b, MHC-II (RT1D), CD29, CD45, CD90 or isotype controls (Figure S8). Cell events were analyzed on a Fortessa cell analyzer (Becton Dickinson, Franklin Lakes, NJ, USA; gating strategy demonstrated in Figure S9) and analyzed using FlowJo Software (FlowJo, LLC, Ashland, OR, USA).

Mixed glial cell culture and microglia isolation

Rat pups (P0-5, mixed gender) were decapitated and the brains were dissected into ice cold HBSS. Meninges were removed and neocortex was dissected out into ice cold HBSS. Tissue was then combined and incubated in 0.25% trypsin plus 50 μ g DNase I for 7 minutes at room temperature and then washed with DMEM plus 10% FBS. Tissue was then washed twice with HBSS and then passed 5 times each through decreasing size serological pipet (10 mL, 5 mL, glass Pasteur pipet) to dissociate the tissue. Tissue suspension was filtered through a 70 μ m cell strainer, spun at 300g for 10 minutes and plated in DMEM plus 10% FBS plus 1% antibiotic-antimycotic (3 brains per T-75 cm² flask) and cultured at 37°C plus 5% CO₂. Media is changed the next day and every 3 days afterwards until confluent. Once confluent, microglia are isolated from mixed

glial population by sealing flasks and shaking at 280 rpm for 30 minutes at 37°C. Microglia-containing media is collected and utilized for downstream applications.

Subventricular zone neural stem cell isolation

4-6-week-old female rats were euthanized via isoflurane overdose and decapitation and the brains were dissected into ice cold HBSS. Brains were cut at the level of the optic chiasm and the subventricular zone was dissected out. Tissue was minced using a scalpel and was transferred to 3 mL of warm media (DMEM/F-12, 20% B27 supplement, 10% N2 supplement, 1% penicillin-streptomycin, 1 mM glutamine, 20 mM KCl, 2 µg/mL heparin) and allowed to settle. Media was aspirated and tissue was resuspended in 1.25 mL 0.1% trypsin-EDTA plus 50 µg DNase I and incubated with agitation for 7 minutes at 37°C. Following incubation, 3 mL of trypsin inhibitor (Sigma-Aldrich #T6522; 139 µg/mL plus 10 µg/mL DNase I in HBSS) and spun at 300g for 5 minutes. Tissue pellet is resuspended in 1 mL of warm media and pipetted 25X with a P1000 pipet set to 800 µL. Media is added to 5 mL and tissue suspension is filtered through a 70 µm cell strainer and spun at 300g for 5 minutes. Cell pellet is resuspended in warm media plus 20 ng/mL EGF + 10 ng/mL bFGF. Growth factors are added every 2 days and media is changed once a week. Neurospheres were passaged using Accumax (Innovative Cell Technologies #AM105) by incubating cells in 1 mL of Accumax for 10 minutes at room temperature on an orbital rotator. Cells were then pipetted 25X with a P1000 pipet set to 900 µL and added to 9 mL of growth media. Cells were then passed through a 70 µm cell strainer, spun at 300g for 5 minutes, and plated for either culture maintenance or for individual experiments.

Oxygen-glucose deprivation

For oxygen-glucose deprivation, cells were dissociated into single cell suspensions, resuspended in 1X HBSS + 1% antibiotic, and plated at appropriate densities. Cells were cultured in 1% oxygen for 4 hours and then transferred back to normal growth conditions.

Oxygen-glucose deprivation effects on cell viability

NSC Cell Counts

NSC were singly dissociated, plated at a concentration of 1000 cells/ μ L and subjected to OGD conditions as described in earlier. After each time point, cells were singly using Accumax (Innovative Cell Technologies #AM105) and counted via hemocytometer.

MTT Assay

For NSCs, cells were plated at a concentration of 1000 cells/ μ L and subjected to OGD conditions as described in earlier. After OGD conditions, 100 μ L of cells were transferred to a 96-well plate. At each time point post OGD, 10 μ L of a 12 mM MTT in PBS solution was added to each well and cells were incubated at 37°C for 48 hours. After incubation, all media was removed, 50 μ L of DMSO was added and incubated at 37°C for 10 mins. Absorbance was read at 595 nm.

For Microglia, 96 well plates were coated with 10 μ g/mL Poly-L-Lysine in sterile tissue culture water for 5 mins and then rinsed 3X with 1X PBS prior to seeding cells. Microglia were plated at concentration 1000 cells/ μ L and let adhere to wells overnight. Microglia were subjected to OGD conditions as described in earlier and after, fresh media was added to wells. At each time point post OGD, 10 μ L of a 12 mM MTT in PBS solution was added to each well and cells

were incubated at 37°C for 24 hours. After incubation, all media was removed, 50 µL of DMSO was added and incubated at 37°C for 10 mins. Absorbance was read at 595 nm.

LDH Assay

For NSCs, cells were plated at a concentration of 1000 cells/µL and subjected to OGD conditions as described in earlier. For LDH media experiments, 50 µL of media was taken at each time point and analyzed as described in the Pierce™ LDH Cytotoxicity Assay Kit (ThermoFisher Scientific, Waltham, MA, USA). For LDH max experiments, 100 µL of media containing cells was collected at each time point and lysed with 10X lysis buffer provided by kit. 50 µL of lysate was then analyzed as described by the kit. Absorbance was read at 450 nm and 620 nm and absorbance were corrected by subtracting 620 nm values from 450 nm.

For Microglia, 96 well plates were coated with 10 µg/mL Poly-L-Lysine in sterile tissue culture water for 5 mins and then rinsed 3X with 1X PBS prior to seeding cells. Microglia were plated at concentration 1000 cells/µL and let adhere to wells overnight. Cells were subjected to OGD conditions as described in earlier. At each time point, 50 µL of media was collected for LDH media experiments and remaining cells were and lysed with 10X lysis buffer provided by kit. Samples were then analyzed according to kit instruction.

TUNEL Assay

For NSCs, 1×10^6 cells were subjected to OGD, collected at each time point and stained with slight modification of NeuroTACS™ II In Situ Apoptosis Detection Kit (Trevigen, Gaithersburg, MD, USA). Streptavidin-488 at a 1:1000 concentration in 1X PBS was used instead of Streptavidin-HRP and DAB solution. Slides were incubated in Streptavidin-488 for

20 minutes at RT, washed 3X in 1X PBS for 10 minutes, stained with DAPI at 1:10,000 in 1X PBS and mounted in PVA-DABCO.

For Microglia, 8-well chamber slides (MilliporeSigma, Burlington, MA, USA) were coated with 10 $\mu\text{L}/\text{mL}$ Matrigel Matrix (Corning, New York, NY, USA) in DMEM for 1 hour at RT followed by 1X PBS wash prior to use. Microglia were plated at 166 cells/ μL and let adhere to wells overnight. Cells were subjected to OGD and stained as described for the NSC TUNEL experiments.

Quantitative reverse transcription polymerase chain reaction

RNA was extracted from cultured cells using the ISOLATE II RNA Mini Kit (Bioline USA, Inc, Taunton, MA, USA) according to manufacturer's instructions and was quantified using a Nanodrop and stored at -80°C until used. cDNA synthesis was performed using the SuperScriptTM III First-Strand Synthesis SuperMix (ThermoFisher Scientific) according to manufacturer's instructions starting with 1 μg total RNA per sample and using oligo(dT) priming and stored at -20°C until used. qPCR was performed using SensiFASTTM SYBR® & Fluorescein Kit (Bioline USA, Inc, Taunton, MA, USA). Each reaction was done using 1 μL of starting cDNA. Relative expression was calculated using the $\Delta\Delta\text{Ct}$ method using RPLP0 as the housekeeping gene. Primer sets are listed in Table S1.

Western blot analysis

Cells were collected and spun at 300g for 5 minutes. The cell pellet was resuspended in RIPA buffer containing protease inhibitor cocktail (1:100, Sigma-Aldrich #P8340) and was sonicated once for 15 seconds at 40% amplitude and then spun at 14,000g for 10 minutes.

Supernatants were collected, quantified via the BCA method, and diluted to 1 $\mu\text{g}/\mu\text{L}$ with lysis buffer and 2X Laemmli sample buffer and boiled for 10 minutes at 95°C with leftover protein being stored at -80°C. 15 μg of each sample was loaded into a 10% Mini-PROTEAN TGX precast gel, run in 1X Tris/Glycine/SDS buffer for 30 minutes at 200V at room temperature and then transferred to nitrocellulose membrane at 100V for 1 hour at 4°C. The membrane was stained with Ponceau S for 5 minutes to confirm protein transfer, destained with 0.1N NaOH and was then washed three times in PBST to remove any trace stain or NaOH. The membrane was then blocked in 5% nonfat milk in 1X PBS plus 0.01% Tween 20 (PBST) for 1 hour at room temperature and incubated for 1 hour at room temperature in primary antibody (Table S2) diluted in PBST. The membrane was then washed three times in PBST and then incubated for 1 hour at room temperature in appropriate secondary antibody (Table S2) diluted in 5% BSA in PBST plus 0.1% NaN_3 . The membrane was then washed three times in PBST followed by once in PBS and imaged using an Odyssey CLx (700 nm or 800 nm channel set to Auto) and protein expression levels were quantified using Image Studio Lite (version 5.2.5; Li-Cor). All protein levels were normalized to levels of actin.

For Western blot analysis of tissue extract, rat brain hemispheres were lysed using the Bio-Plex Cell Lysis Kit (Bio-Rad, Inc) according to manufacturer's instructions, quantified using the BCA method, and diluted to 3 $\mu\text{g}/\mu\text{L}$ with lysis buffer and 2X Laemmli sample buffer and boiled for 10 minutes at 95°C with leftover protein being stored at -80°C. SDS-PAGE and Western blot was performed as above using 30 μg of total protein per sample.

BrdU Flow Cytometry

Cell cycle analysis was done utilizing a FITC BrdU Flow Kit (BD Biosciences) according to manufacturer's instructions. Briefly, neural stem cells were singly dissociated and plated in either normal growth media, nMSC conditioned media, or aMSC γ conditioned media and allowed to grow for 24, 48, or 72 hours. 4 hours prior to fixation, BrdU (10 μ M final concentration) was added to each well to label dividing cells. At appropriate time points, cells were fixed and permeabilized, and treated with DNase I to expose the incorporated BrdU. Cells were then incubated with a FITC-conjugated anti-BrdU antibody and labeled with 7-AAD. Cell events were analyzed on a Fortessa cell analyzer (Becton Dickinson, Franklin Lakes, NJ, USA; gating strategy demonstrated in Figure S9) and analyzed using FlowJo Software (FlowJo, LLC, Ashland, OR, USA).

Magnetic resonance imaging

Image Acquisition

48 hours after surgery, animals were anesthetized using isoflurane and magnetic resonance imaging was performed using an Agilent 9.4T MR system (Agilent Technologies, Santa Clara, CA), with a 600 mT/m gradient insert, a 72 mm ID active decoupling birdcage RF coil for transmission, and a 4-channel phase array coil as the receiver (Rapid Biomed, Ripmar, Germany). In each animal, T1-, T2-, and diffusion-weighted MR images were acquired, using spin echo multi slice (SEMS) sequences. For the T1 sequence, imaging settings were as follows: TR/TE = 555/13 ms, FOV = 40X40 mm, Averages = 6, matrix = 256X256, slice thickness = 1.0 mm, gap = 0 mm. For the T2 sequence, imaging settings were as follows: TR/TE = 2000/45 ms, FOV = 40X40 mm, Averages = 4, matrix = 256X256, slice thickness = 1.0 mm, gap = 0 mm. For the diffusion weighted imaging (DWI) sequence, imaging settings were as follows: TR/TE = 2000/45 ms, FOV = 40X40

mm, Averages = 2, matrix = 128X128, slice thickness = 1.0 mm, gap = 0 mm, two *b*-values of 0 and 650 s/mm², diffusion separation $\Delta = 25$ ms, diffusion gradient duration $\delta = 5$ ms.

Infarct Volume calculation

Infarct volume and percent infarction were calculated using the DWI MRI sequences. Correcting for edema, these were calculated as follows:

$$\text{Infarct Volume (mm}^3\text{)} = \sum_1^n \text{InV}_n - (\text{IpV}_n - \text{CoV}_n)$$

$$\text{Percent Infarction (\%)} = 100 * \frac{\sum_1^n \text{InV}_n}{\sum_1^n (\text{IpV}_n + \text{CoV}_n)}$$

Where the individual slice infarct volume is InV, the individual slice ipsilateral hemisphere volume is IpV, individual slice contralateral hemisphere volume is CoV, and n is the slice number.

Functional testing after MCAO

Modified Neurological Severity Score

Animals were scored using the modified neurological severity score (mNSS) as previously described⁶⁰. Scores were obtained at baseline before surgery and on postoperative days 1-7, 14, and 21. The mNSS is a cumulative scoring system that combines motor, sensory, balance, and reflex deficits. One point is given for an inability to perform a motor or sensory task and one point is given for the absence of one of the reflexes. The section scores are summed for a maximum score of 18, with higher scores indicating a more impaired animal.

Open Field Testing

Animals were tested in an open field apparatus (Med Associates, Inc) for 15 minutes 24 hours and 7 days after surgery. Center/periphery analysis and rotational analysis were done using predetermined configurations in the corresponding Activity Monitor Software package (Med Associates, Inc).

Brain processing

At appropriate time points, rats were euthanized via isoflurane overdose followed by transcardial perfusion with ice cold heparinized saline (10 U/mL) for 12 minutes and with ice cold 4% paraformaldehyde for 15 minutes. Brains were then removed and post-fixed in PFA for 16 hours at 4°C, washed once in 1X PBS, and transferred to 30% sucrose until they sunk. Brains were then sectioned at 50 µm and stored in cryoprotectant (47.6% 1X PBS, 28.6% ethylene glycol, 23.8% glycerol) at -20°C.

Immunofluorescence staining

Tissue sections were washed three times at room temperature in 1X TBS for 5 minutes each. Tissue was then blocked in blocking buffer (1X TBS, 0.3M glycine, 5% normal donkey serum, 0.25% Triton X-100) for 2 hours at room temperature and then incubated in primary antibody (Table S2), diluted in blocking buffer, for 72 hours at 4°C. Tissue was then washed three times at room temperature in 1X TBS for 5 minutes each and incubated in secondary antibody (Table S2), diluted in blocking buffer, for 2 hours at room temperature. Tissue was then washed three times at room temperature in 1X TBS for 5 minutes each and incubated in DAPI (0.5 µg/mL; ThermoFisher Scientific #D1306) or TO-PRO-3 Iodide (1 µM; ThermoFisher Scientific #T3605) for 5 minutes at room temperature and then mounted and stored at 4°C. For sections that were

stained for BrdU, tissue was washed three times at room temperature in 1X TBS for 5 minutes each then incubated in 2N HCl at 37°C for 30 minutes. Afterwards, tissue was incubated in 0.1M borate buffer for 10 minutes at room temperature, washed six times at room temperature in 1X TBS for 5 minutes each, and stained as above.

Stereological quantification

Cell counts were performed using design-based stereology (StereoInvestigator, MBF Biosciences). For the analysis, every sixth section of brain tissue was quantified using the optical fractionator workflow of StereoInvestigator. Regions of interest were traced under 5X magnification with counting performed under 63X magnification with a counting frame of 225 µm x 145 µm and sampling grid of 100 µm x 100 µm with 12.5 µm top and bottom guard zones.

Quantification of CD68 staining

To quantify level of microglia activity, tissue sections were stained for CD68 and were imaged using a Zeiss AxioImager with a 10X objective and were tiled in AxioVision (Carl Zeiss). Intensity analysis was performed in ImageJ. On each section, the intensity of the region of interest was measured as well as three background regions. CD68 staining was background corrected and normalized to measured area according to the following formula:

$$CD68\ Intensity = \frac{\sum_1^n (Int_{ROI})_n - (\bar{x}_{BackInt})_n}{\sum_1^n Area_n}$$

Where Int_{ROI} is the intensity of the defined region of interest, $\bar{x}_{BackInt}$ is the average of the background intensity, $Area$ is the measured area of the region of interest, and n is the section number.

Quantification of striatal CNPase and PDGFR α

For each animal, 3 to 4 randomly selected fields (280 x 280 μm) from the striatum in 4 sections with 300 μm separating each section were acquired using a Zeiss LSM 880 confocal microscope with Airyscan detector. Forty-eight micron maximum projection z-stacks were reconstructed and the number of CNPase-positive and PDGFR α -positive cells per mm^2 were determined using the ImageJ Cell Counter plugin analysis tool.

***In vitro* cytokine analysis**

100,000 primary rat microglia were plated in triplicate per well of a 96 well plate and grown in oxygen-glucose deprivation or normal growth conditions for 4 hours. After 4 hours, media was replaced with the normal growth media, nMSC conditioned media, or aMSC γ conditioned media. Supernatants were collected 24 hours, 48 hours, 4 days, or 7 days later and stored at -80°C until analyzed. Cytokines levels were determined using the Rat Proinflammatory Panel 2 V-PLEX Assay (Meso Scale Discovery) according to manufacturer's instructions.

Mass spectrometry

Sample preparation, TMT labeling, and fractionation

15 mL of conditioned media was collected as above and concentrated using an Amicon Ultra-15 centrifugal filter unit with a 3 kDa molecular weight cutoff (Millipore, Burlington, MA, USA). Concentrated protein was quantified using a BCA protein assay kit (ThermoFisher Scientific, Waltham, MA, USA) and 100 μg of total protein from each sample was processed by filter aided sample preparation. Proteins were diluted in 8 M urea, reduced in 5 mM DTT in 8 M urea for 20 minutes at 55°C and then alkylated in 10 mM iodoacetamide for 20 minutes at room

temperature in the dark. The samples were then urea exchanged with 50 mM triethylammonium bicarbonate (TEAB) and trypsin (2 µg per sample) was added and samples were incubated overnight at 37°C. Peptides were eluted with 80 µL of 50 mM TEAB and then digested peptides were labeled using 2 tandem mass tag (TMT) kits (ThermoFisher Scientific) according to manufacturer's instructions where samples were labeled using 126-131 tags (one replicate per mass tag). Subsequently, the individual samples were combined, lyophilized, and resuspended in 10 mM ammonium hydroxide and fractionated (20 fractions) via high pH reverse phase chromatography. Each fraction was then lyophilized and resuspended in 20 µL 0.1% formic acid prior to nano-LC-MS/MS

Nano-LC-MS/MS analysis and data analysis

Mass detection occurred with an Orbitrap Velos Pro (ThermoFisher Scientific) equipped with an Agilent HPLC system. Chromatographic separation of peptides was accomplished using a Zorbax 300SB-C18 column (3.5 µm ID x 150 mm, particle size 5 µm, pore size 100 Å, Agilent Technologies). The peptides were loaded onto a Zorbax 300SB-C18 trap cartridge at a flow rate of 3 µL/minute for 10 minutes. After washing with 0.1% formic acid, the peptides were eluted using a 5-40% B gradient for 60 minutes at a flow rate of 250 nL/minute acid (mobile phase A = 0.1% formic acid; mobile phase B = 0.1% formic acid in acetonitrile). The flow-through was analyzed using DDA settings to select the top 10 most abundant ions for HCD fragmentation. Proteins were identified by searching MS/MS spectra against the Human SwissProt database using the Mascot search engine employing a reversed decoy database to calculate the false discovery rate (FDR). Trypsin was set as the protease with two missed cleavages and searches were performed with precursor and fragment mass error tolerances were set at 15 ppm and 0.4 Da,

respectively. Peptide precursors of +2, +3, and +4 were considered. Peptide variable modifications allowed during the search were: oxidation (M) and deamination (NQ), whereas carbamidomethyl (C) and TMT6plex (K and N-term) were set as fixed modifications. To calculate the FDR, the search was performed using the “decoy” option in Mascot. Scaffold Q+ was used to quantitate TMT-labeled peptides from the samples. Peptide identifications were accepted if they could be established at a greater than 95.0% probability by the Scaffold Local FDR algorithm. Protein identifications were accepted if they could be established at a greater than 99.0% probability and contained at least 2 identified peptides. Protein probabilities were assigned by the Protein Prophet algorithm. Proteins that contained similar peptides and could not be differentiated based on MS/MS analysis alone were grouped to satisfy the principles of parsimony. Proteins sharing significant peptide evidence were grouped into clusters. Normalization was performed iteratively (across samples and spectra) on intensities. Medians were used for averaging. Spectra data were log-transformed, pruned of those matched to multiple proteins, and weighted by an adaptive intensity weighting algorithm. Pathway analyses were conducted using the PANTHER database (www.pantherdb.org) and the DAVID Gene Functional Classification Tool (<https://david.ncifcrf.gov>). Differentially expressed proteins for MetaCore (Thomson Reuters) pathway enrichment were determined by applying Permutation Test with unadjusted significance level $p < 0.05$ corrected by Benjamini-Hochberg (new $p < 0.008$) and a minimum fold change of ± 1 (Table S3,S4).

Data availability

Datasets generated or analyzed for these studies are available from the corresponding author upon reasonable request. Mass spectrometry proteomics data have been deposited to the

ProteomeXchange Consortium via the MassIVE repository with the dataset identifier MSV000082984. Figure 6 and Tables S3 and S4 were generated from these data.

Table S1. Primer sequences for qRT-PCR.

Gene	Forward	Reverse	RefSeq No.
GDNF	CGAAGAGAGAGGAACCG	TAGCCCAAACCCAAGTC	NM_019139.1
IGF-1	TACTTCAACAAGCCCACAG	TACATCTCCAGCCTCCTC	NM_001082478.1
BDNF	ACCCTGAGTTCCACCAG	AAGTTGCCTTGTCCGTG	NM_001270630.1
NTF3	TAATGATGAGTGGCTGCG	CCGTATGACTATTTCCAGGG	NM_031073.3
NGF	CGCATCGCTCTCCTTCA	GCCCAGACACTGAGGTG	NM_001277055.1
RPLP0	TTCTCCTTCGGGCTGAT	ATTGCGGACACCCTCTA	NM_022402.2

All primer sets used in this dissertation were designed against rat genes. GDNF – glial derived neurotrophic factor; IGF-1 – insulin-like growth factor 1; BDNF – brain derived neurotrophic factor; NTF3 – neurotrophin 3; NGF – nerve growth factor; RPLP0 – ribosomal protein lateral stalk subunit P0.

Table S2. Antibodies.

Target	Conjugate	Supplier	Catalog No.	Application(s)	Concentration
Sox2	-	Santa Cruz	sc-17320	WB	0.4 µg/mL
GFAP	-	Dako	Z0334	WB	5.8 µg/mL
PDGFRα	-	Santa Cruz	sc-338	IHC WB	0.4 µg/mL 0.2 µg/mL
Actin	-	ThermoFisher Scientific	MA5-11869	WB	0.04 µg/mL
B-III-tubulin	-	ThermoFisher Scientific	32-2600	WB	0.1 µg/mL
BrdU	-	Abcam	ab6326	IHC	2 µg/mL
DCX	-	Santa Cruz	sc-8066	IHC WB	0.2 µg/mL 0.2 µg/mL
Cyclin D1	-	Abcam	ab74646	WB	5 µg/mL
Iba1	-	Wako	019-19741	IHC	0.5 µg/mL
CD68	-	Bio-Rad	MCA341R	IHC	2 µg/mL
CNPase	-	Gift from Dr. Ernesto Bongarzone	-	IHC	1:10 dilution
MBP	-	Santa Cruz	sc-376995	WB	0.4 µg/mL
CD11b	Biotin	BioLegend	201803	MSC Purification	10 µg/mL
CD45	Biotin	BioLegend	202203	MSC Purification	10 µg/mL
CD11b	V450	BD Biosciences	562108	FC	0.5 µg/test
RT1D	FITC	BD Biosciences	550982	FC	0.5 µg/test
CD29	PE	BD Biosciences	562154	FC	0.5 µg/test
CD45	PE-Cy7	BD Biosciences	561588	FC	0.5 µg/test
CD90	APC	eBioscience	17-0900	FC	0.5 µg/test
Ms IgA	V450	BD Biosciences	5262142	FC	0.5 µg/test
Ms IgG1	FITC	BD Biosciences	550616	FC	0.5 µg/test
Hm IgM	PE	BD Biosciences	562114	FC	0.5 µg/test
Ms IgG1	PE-Cy7	BD Biosciences	561588	FC	0.5 µg/test
Ms IgG2a	APC	eBioscience	17-4724	FC	0.5 µg/test
Rabbit IgG	IRDye 800CW	LI-COR	925-32213	WB	0.05 µg/mL
Goat IgG	IRDye 800 CW	LI-COR	925-32214	WB	0.05 µg/mL
Mouse IgG	IRDye 680RD	LI-COR	925-68072	WB	0.05 µg/mL
Mouse IgG	IRDye 680LT	LI-COR	925-68022	WB	0.05 µg/mL
Rabbit IgG	Biotin	Jackson ImmunoResearch	711-065-152	IHC	6 µg/mL

Streptavidin	AF488	Jackson ImmunoResearch	016-540-084	IHC	1.5 µg/mL
Goat IgG	AF488	Jackson ImmunoResearch	705-545-147	IHC	3 µg/mL
Rat IgG	Cy3	Jackson ImmunoResearch	712-165-153	IHC	3 µg/mL
Rabbit IgG	Cy3	Jackson ImmunoResearch	711-585-152	IHC	3 µg/mL
Mouse IgG	Cy3	Jackson ImmunoResearch	715-165-151	IHC	3 µg/mL
Goat IgG	Cy5	Jackson ImmunoResearch	705-175-147	IHC	6 µg/mL

Primary antibodies are listed above the black line and secondary antibodies are listed below the black line. Sox2 – SRY box 2; GFAP – glial fibrillary acidic protein; PDGFR α – platelet derived growth factor receptor α ; BrdU – 5-bromo-2'-deoxyuridine; DCX – doublecortin; Iba1 – ionized calcium-binding adapter molecule 1; CD – cluster of differentiation; RT1D – MHC class II RT1D alpha chain; Ig – immunoglobulin; Ms – mouse; Hm – hamster; WB – Western blot; IHC – immunohistochemistry; MSC – mesenchymal stem cell; FC – flow cytometry.

Table S3. Proteins identified by mass spectrometry.

Protein Descriptions	UniProt Accession ID	Gene Symbol
72 kDa type IV collagenase OS=Rattus norvegicus GN=Mmp2 PE=2 SV=2	P33436	Mmp2
78 kDa glucose-regulated protein OS=Rattus norvegicus GN=Hspa5 PE=1 SV=1	P06761	Hspa5
A disintegrin and metalloproteinase with thrombospondin motifs 1 OS=Rattus norvegicus GN=Adamts1 PE=2 SV=1	Q9WUQ1	Adamts1
Actin, aortic smooth muscle OS=Rattus norvegicus GN=Acta2 PE=2 SV=1	P62738	Acta2
Actin, beta-like 2 OS=Rattus norvegicus GN=Actb12 PE=1 SV=1	D3ZRN3	γ Actb12
Actinin alpha 2 OS=Rattus norvegicus GN=Actn2 PE=1 SV=1	D3ZCV0	Actn2
Actinin alpha 3 OS=Rattus norvegicus GN=Actn3 PE=1 SV=1	Q8R4I6	ⁿ Actn3
Actn1 protein OS=Rattus norvegicus GN=Actn1 PE=1 SV=1	Q6GMN8	Actn1
ADAM metalloproteinase with thrombospondin type 1 motif, 12 OS=Rattus norvegicus GN=Adamts12 PE=4 SV=2	D3ZTJ3	Adamts12
ADAMTS-like 3 OS=Rattus norvegicus GN=Adamts13 PE=4 SV=3	D4ADD4	Adamts13
Adipocyte enhancer-binding protein 1 OS=Rattus norvegicus GN=Aebp1 PE=2 SV=1	A2RUV9	Aebp1
Aggrecan core protein OS=Rattus norvegicus GN=Acan PE=1 SV=2	P07897; D4A7Y1	Acan
AHNAK nucleoprotein OS=Rattus norvegicus GN=Ahnak PE=1 SV=1	A0A0G2JU96	ⁿ Ahnak
Alpha 4 type V collagen OS=Rattus norvegicus GN=Col5a3 PE=2 SV=1	Q9JI04	Col5a3
Alpha-1-macroglobulin OS=Rattus norvegicus GN=A1m PE=1 SV=1	Q63041	A1m
Alpha-2 antiplasmin OS=Rattus norvegicus GN=Serpinf1 PE=1 SV=1	Q80ZA3	Serpinf1
Alpha-2-macroglobulin OS=Rattus norvegicus GN=A2m PE=2 SV=2	P06238	A2m
Alpha-actinin-4 OS=Rattus norvegicus GN=Actn4 PE=1 SV=2	Q9QXQ0	Actn4
Alpha-internexin OS=Rattus norvegicus GN=Ina PE=1 SV=2	P23565;G3V8Q2	ⁿ Ina
Amyloid beta A4 protein OS=Rattus norvegicus GN=App PE=1 SV=2	P08592	App
Apolipoprotein B-100 OS=Rattus norvegicus GN=Apob PE=1 SV=1	Q7TMA5	Apob
Beta-2-glycoprotein 1 OS=Rattus norvegicus GN=Apoh PE=2 SV=2	P26644	Apoh
Beta-2-microglobulin OS=Rattus norvegicus GN=B2m PE=1 SV=1	P07151	B2m
Biglycan OS=Rattus norvegicus GN=Bgn PE=2 SV=1	P47853	Bgn
C1r protein OS=Rattus norvegicus GN=C1r PE=1 SV=1	B5DEH7	C1r
Cadherin 13 OS=Rattus norvegicus GN=Cdh13 PE=2 SV=1	Q8R490	Cdh13
Calreticulin OS=Rattus norvegicus GN=Calr PE=1 SV=1	P18418	Calr
Protein Descriptions	UniProt Accession ID	Gene Symbol
Calsequestrin OS=Rattus norvegicus GN=Casq2 PE=1 SV=2	F1M944	Casq2
Calsyntenin-1 OS=Rattus norvegicus GN=Clstn1 PE=2 SV=1	Q6Q0N0	Clstn1
Carboxypeptidase E OS=Rattus norvegicus GN=Cpe PE=1 SV=1	P15087;D4A8X4	Cpe
Carboxypeptidase OS=Rattus norvegicus GN=Ctsa PE=1 SV=1	Q6AYS3	ⁿ Ctsa
Carboxypeptidase Q OS=Rattus norvegicus GN=Cpq PE=1 SV=1	Q6IRK9	Cpq

Cartilage oligomeric matrix protein OS=Rattus norvegicus GN=Comp PE=1 SV=1	P35444	Comp
Catenin beta-1 OS=Rattus norvegicus GN=Ctnnb1 PE=1 SV=1	Q9WU82	ⁿ Ctnnb1
Cathepsin B OS=Rattus norvegicus GN=Ctsb PE=1 SV=1	Q6IN22	Ctsb
Cathepsin L1 OS=Rattus norvegicus GN=Ctsl PE=1 SV=2	P07154	Ctsl
CD44 antigen OS=Rattus norvegicus GN=Cd44 PE=1 SV=2	P26051	Cd44
Chondroitin sulfate proteoglycan 4 OS=Rattus norvegicus GN=Cspg4 PE=1 SV=2	Q00657	Cspg4
Class I histocompatibility antigen, Non-RT1.A alpha-1 chain OS=Rattus norvegicus GN=RT1-Aw2 PE=1 SV=1	P15978	^γ RT1-Aw2
Coiled-coil domain-containing protein 80 OS=Rattus norvegicus GN=Ccdc80 PE=1 SV=1	Q6QD51	Ccdc80
Collagen alpha-1(I) chain OS=Rattus norvegicus GN=Col1a1 PE=1 SV=5	P02454	Col1a1
Collagen alpha-1(II) chain OS=Rattus norvegicus GN=Col2a1 PE=1 SV=2	P05539	Col2a1
Collagen alpha-1(III) chain OS=Rattus norvegicus GN=Col3a1 PE=2 SV=3	P13941	Col3a1
Collagen alpha-1(V) chain OS=Rattus norvegicus GN=Col5a1 PE=1 SV=1	Q9JI03;A0A0G2JX47	Col5a1
Collagen alpha-1(XI) chain OS=Rattus norvegicus GN=Col11a1 PE=1 SV=2	P20909	Col11a1
Collagen alpha-1(XII) chain (Fragment) OS=Rattus norvegicus GN=Col12a1 PE=2 SV=1	P70560;A0A0G2KAJ7	Col12a1
Collagen alpha-2(I) chain OS=Rattus norvegicus GN=Col1a2 PE=1 SV=3	P02466;A0A0G2K5E8	Col1a2
Collagen type IV alpha 1 chain OS=Rattus norvegicus GN=Col4a1 PE=1 SV=1	F1MA59	Col4a1
Collagen type IV alpha 2 chain OS=Rattus norvegicus GN=Col4a2 PE=1 SV=3	F1M6Q3	Col4a2
Collagen type IV alpha 5 chain OS=Rattus norvegicus GN=Col4a5 PE=3 SV=3	F1LUN5	Col4a5
Collagen type V alpha 2 chain OS=Rattus norvegicus GN=Col5a2 PE=1 SV=3	F1LQ00	Col5a2
Collagen type VI alpha 1 chain OS=Rattus norvegicus GN=Col6a1 PE=1 SV=1	D3ZUL3	Col6a1
Collagen type VI alpha 2 chain OS=Rattus norvegicus GN=Col6a2 PE=1 SV=2	F1LNH3	Col6a2
Collagen type VIII alpha 1 chain OS=Rattus norvegicus GN=Col8a1 PE=1 SV=3	D4AC70	Col8a1
Protein Descriptions	UniProt Accession ID	Gene Symbol
Collagen type VIII alpha 2 chain OS=Rattus norvegicus GN=Col8a2 PE=4 SV=1	D4ADG9	Col8a2
Collagen type XV alpha 1 chain OS=Rattus norvegicus GN=Col15a1 PE=1 SV=1	A0A0G2JV12	Col15a1
Collagen type XVI alpha 1 chain OS=Rattus norvegicus GN=Col16a1 PE=1 SV=2	F1LND0	Col16a1
Collagen type XVIII alpha 1 chain OS=Rattus norvegicus GN=Col18a1 PE=1 SV=2	F1LR02	Col18a1
Complement C1q tumor necrosis factor-related protein 5 OS=Rattus norvegicus GN=C1qtnf5 PE=2 SV=1	Q5FVH0	C1qtnf5
Complement C1s subcomponent OS=Rattus norvegicus GN=C1s PE=1 SV=1	G3V7L3;D4A1S0	^γ C1s

Complement C2 OS=Rattus norvegicus GN=C2 PE=1 SV=1	Q6MG73;A0A0U1RRP9	C2
Complement C3 OS=Rattus norvegicus GN=C3 PE=1 SV=3	P01026;M0RBF1	C3
Complement C4B (Chido blood group) OS=Rattus norvegicus GN=C4b PE=1 SV=1	Q6MG90	C4b
Complement component 4A (Rodgers blood group) OS=Rattus norvegicus GN=C4a PE=1 SV=2	M0RB00	C4a
Connective tissue growth factor OS=Rattus norvegicus GN=Ctgf PE=2 SV=1	Q9R1E9	Ctgf
Cystatin-C OS=Rattus norvegicus GN=Cst3 PE=1 SV=2	P14841	Cst3
Cysteine and glycine-rich protein 1 OS=Rattus norvegicus GN=Csrp1 PE=1 SV=2	P47875	ⁿ Csrp1
Desmin OS=Rattus norvegicus GN=Des PE=1 SV=2	P48675	Des
Dystroglycan 1 OS=Rattus norvegicus GN=Dag1 PE=1 SV=1	F1M8K0	Dag1
EGF-containing fibulin-like extracellular matrix protein 2 OS=Rattus norvegicus GN=Efemp2 PE=1 SV=1	A0A0G2K2R5	Efemp2
Elastin microfibril interfacier 1 OS=Rattus norvegicus GN=Emilin1 PE=1 SV=1	D3Z9E1	Emilin1
Elastin OS=Rattus norvegicus GN=Eln PE=1 SV=2	Q99372	Eln
Elongation factor 1-alpha 1 OS=Rattus norvegicus GN=Eef1a1 PE=2 SV=1	P62630	Eef1a1
Elongation factor 1-alpha 2 OS=Rattus norvegicus GN=Eef1a2 PE=1 SV=1	P62632	^γ Eef1a2
Elongation factor 2 OS=Rattus norvegicus GN=Eef2 PE=1 SV=4	P05197	Eef2
Endothelial differentiation-related factor 1 OS=Rattus norvegicus GN=Edf1 PE=1 SV=1	P69736	Edf1
Extracellular matrix protein 1 OS=Rattus norvegicus GN=Ecm1 PE=1 SV=2	Q62894	Ecm1
Extracellular sulfatase Sulf-1 OS=Rattus norvegicus GN=Sulf1 PE=1 SV=1	Q8VI60	Sulf1
FAT atypical cadherin 1 OS=Rattus norvegicus GN=Fat1 PE=1 SV=1	A0A0G2K5L1	Fat1
Fibrillin 1 OS=Rattus norvegicus GN=Fbn1 PE=1 SV=1	G3V9M6	Fbn1
Fibrillin 2 OS=Rattus norvegicus GN=Fbn2 PE=4 SV=3	F1M5Q4	Fbn2
Protein Descriptions	UniProt Accession ID	Gene Symbol
Fibronectin OS=Rattus norvegicus GN=Fn1 PE=1 SV=3	F1LST1;A0A096P6L8	Fn1
Fibulin 2 OS=Rattus norvegicus GN=Fbln2 PE=1 SV=1	G3V6X1	Fbln2
Fibulin-1 OS=Rattus norvegicus GN=Fbln1 PE=1 SV=1	D3ZQ25	Fbln1
Fibulin-5 OS=Rattus norvegicus GN=Fbln5 PE=2 SV=1	Q9WVH8	Fbln5
Filamin A OS=Rattus norvegicus GN=Flna PE=1 SV=1	C0JPT7	Flna
Follistatin-related protein 1 OS=Rattus norvegicus GN=Fstl1 PE=1 SV=1	Q62632;F8WG88	Fstl1
Follistatin-related protein 3 OS=Rattus norvegicus GN=Fstl3 PE=2 SV=1	Q99PW7	Fstl3
Fructose-bisphosphate aldolase OS=Rattus norvegicus GN=Aldoat2 PE=2 SV=1	Q6AY07	Aldoat2
Galectin-3-binding protein OS=Rattus norvegicus GN=Lgals3bp PE=1 SV=2	O70513	Lgals3bp
Gelsolin OS=Rattus norvegicus GN=Gsn PE=1 SV=1	Q68FP1	Gsn
Gliomedin OS=Rattus norvegicus GN=Gldn PE=1 SV=1	Q80WL1	ⁿ Gldn

Glyceraldehyde-3-phosphate dehydrogenase, testis-specific OS=Rattus norvegicus GN=Gapdhs PE=1 SV=1	Q9ESV6	ⁿ Gapdhs
Glypican 4 OS=Rattus norvegicus GN=Gpc4 PE=1 SV=1	Q642B0	Gpc4
GM2 ganglioside activator OS=Rattus norvegicus GN=Gm2a PE=1 SV=1	Q6IN37	Gm2a
Granulin, isoform CRA_c OS=Rattus norvegicus GN=Grn PE=4 SV=1	G3V8V1	Grn
Haptoglobin OS=Rattus norvegicus GN=Hp PE=1 SV=3	P06866	Hp
Heat shock protein HSP 90-alpha OS=Rattus norvegicus GN=Hsp90aa1 PE=1 SV=3	P82995	Hsp90aa1
Heat shock protein HSP 90-beta OS=Rattus norvegicus GN=Hsp90ab1 PE=1 SV=4	P34058	^γ Hsp90ab1
Hemicentin 1 OS=Rattus norvegicus GN=Hmcn1 PE=1 SV=3	F1M4Q3	Hmcn1
Hepatoma-derived growth factor-related protein 3 OS=Rattus norvegicus GN=Hdgfrp3 PE=1 SV=1	Q923W4	Hdgfr3
Heterogeneous nuclear ribonucleoprotein K OS=Rattus norvegicus GN=Hnrnpk PE=1 SV=1	P61980	^γ Hnrnpk
Histone cluster 1 H1 family member c OS=Rattus norvegicus GN=Hist1h1c PE=1 SV=1	A0A0G2K654	Hist1h1c
Histone H1.0 OS=Rattus norvegicus GN=H1f0 PE=2 SV=2	P43278	H1f0
Histone H1.1 OS=Rattus norvegicus GN=Hist1h1a PE=1 SV=1	D4A3K5	Hist1h1a
Histone H1.4 OS=Rattus norvegicus GN=Hist1h1e PE=1 SV=3	P15865	Hist1h1e
Histone H1.5 OS=Rattus norvegicus GN=Hist1h1b PE=1 SV=1	D3ZBN0	Hist1h1b
Histone H1t OS=Rattus norvegicus GN=Hist1h1t PE=1 SV=2	P06349	Hist1h1t
Protein Descriptions	UniProt Accession ID	Gene Symbol
Histone H2B OS=Rattus norvegicus GN=Hist1h2bo PE=3 SV=1	A0A0G2JXI9	Hist1h2bo
Histone H2B OS=Rattus norvegicus GN=Hist2h2be PE=3 SV=3	D4A817	^γ Hist2h2be
Histone H2B OS=Rattus norvegicus GN=LOC102549061 PE=3 SV=1	A0A0G2JXE0	^γ LOC102549061
Inactive serine protease 35 OS=Rattus norvegicus GN=Prss35 PE=2 SV=1	Q5R212	Prss35
Insulin-like growth factor binding protein 7, isoform CRA_b OS=Rattus norvegicus GN=Igfbp7 PE=1 SV=2	F1M9B2	Igfbp7
Inter-alpha-trypsin inhibitor heavy chain H3 OS=Rattus norvegicus GN=Itih3 PE=2 SV=1	Q63416	Itih3
Interleukin-1 receptor-like 1 OS=Rattus norvegicus GN=Il1rl1 PE=2 SV=1	Q62611;F1LR63	Il1rl1
Lactadherin OS=Rattus norvegicus GN=Mfge8 PE=2 SV=1	P70490;Q1PBJ1	Mfge8
Laminin subunit alpha 4 OS=Rattus norvegicus GN=Lama4 PE=1 SV=3	F1LTF8	Lama4
Laminin subunit alpha 5 OS=Rattus norvegicus GN=Lama5 PE=1 SV=2	F1MAN8	Lama5
Laminin subunit beta 1 OS=Rattus norvegicus GN=Lamb1 PE=1 SV=3	D3ZQN7	Lamb1
Laminin subunit beta-2 OS=Rattus norvegicus GN=Lamb2 PE=2 SV=1	P15800	Lamb2
Laminin subunit gamma 1 OS=Rattus norvegicus GN=Lamc1 PE=1 SV=1	F1MAA7	Lamc1
Latent-transforming growth factor beta-binding protein 1 OS=Rattus norvegicus GN=Ltbp1 PE=1 SV=1	Q00918	Ltbp1
Latent-transforming growth factor beta-binding protein 2 OS=Rattus norvegicus GN=Ltbp2 PE=1 SV=1	O35806;A0A0G2K1G5	Ltbp2
Latent-transforming growth factor beta-binding protein 3 OS=Rattus norvegicus GN=Ltbp3 PE=4 SV=1	F1LRT0	Ltbp3

Lipocalin 7, isoform CRA_a OS=Rattus norvegicus GN=Timag11 PE=1 SV=1	Q4V8N0;Q9EQT5	Timag11
L-lactate dehydrogenase A chain OS=Rattus norvegicus GN=Ldha PE=1 SV=1	P04642	Ldha
L-lactate dehydrogenase B chain OS=Rattus norvegicus GN=Ldhb PE=1 SV=2	P42123	Ldhb
Lumican OS=Rattus norvegicus GN=Lum PE=1 SV=1	P51886	Lum
Lysyl oxidase homolog 2 OS=Rattus norvegicus GN=Loxl2 PE=2 SV=2	B5DF27;A0A0G2K4P0	Loxl2
Lysyl oxidase-like 1 OS=Rattus norvegicus GN=Loxl1 PE=2 SV=1	Q5FWS5	Loxl1
Lysyl oxidase-like 3 OS=Rattus norvegicus GN=Loxl3 PE=4 SV=1	D3ZP82	Loxl3
Lysyl oxidase-like 4 OS=Rattus norvegicus GN=Loxl4 PE=4 SV=1	D4A9V5	Loxl4
Macrophage colony-stimulating factor 1 OS=Rattus norvegicus GN=Csf1 PE=2 SV=1	Q8JZQ0	Csf1
Mannan-binding lectin serine protease 1 OS=Rattus norvegicus GN=Masp1 PE=1 SV=2	Q8CHN8	Masp1
Matrix Gla protein OS=Rattus norvegicus GN=Mgp PE=1 SV=2	P08494	Mgp
Protein Descriptions	UniProt Accession ID	Gene Symbol
Matrix metalloproteinase 19 OS=Rattus norvegicus GN=Mmp19 PE=2 SV=1	C0M4B0	ⁿ Mmp19
Matrix metalloproteinase-14 OS=Rattus norvegicus GN=Mmp14 PE=2 SV=2	Q10739	Mmp14
Matrix metalloproteinase-23 OS=Rattus norvegicus GN=Mmp23 PE=1 SV=1	O88272	Mmp23
Mesothelin OS=Rattus norvegicus GN=Msln PE=2 SV=2	Q9ERA7	Msln
Metalloendopeptidase OS=Rattus norvegicus GN=Bmp1 PE=3 SV=2	F1M798	Bmp1
Metalloendopeptidase OS=Rattus norvegicus GN=Tll1 PE=3 SV=3	D3Z8U5	Tll1
Metalloproteinase inhibitor 1 OS=Rattus norvegicus GN=Timp1 PE=1 SV=2	P30120	Timp1
Metalloproteinase inhibitor 2 OS=Rattus norvegicus GN=Timp2 PE=1 SV=3	P30121	Timp2
Multiple inositol polyphosphate phosphatase 1 OS=Rattus norvegicus GN=Minpp1 PE=1 SV=3	O35217	Minpp1
Myosin, heavy polypeptide 9, non-muscle OS=Rattus norvegicus GN=Myh9 PE=1 SV=1	G3V6P7;Q62812	Myh9
Neurofilament heavy polypeptide OS=Rattus norvegicus GN=Nefh PE=1 SV=4	P16884;F1LRZ7	Nefh
Neurofilament light polypeptide OS=Rattus norvegicus GN=Nefl PE=1 SV=3	P19527	^γ Nefl
Neurofilament medium polypeptide OS=Rattus norvegicus GN=Nefm PE=1 SV=3	G3V7S2	Nefm
Nidogen-1 OS=Rattus norvegicus GN=Nid1 PE=1 SV=1	F1LM84	Nid1
Nidogen-2 OS=Rattus norvegicus GN=Nid2 PE=2 SV=1	B5DFC9	Nid2
Non-muscle caldesmon OS=Rattus norvegicus GN=Cald1 PE=1 SV=1	Q62736;A0A0G2JTV2	Cald1
NPC intracellular cholesterol transporter 2 OS=Rattus norvegicus GN=Npc2 PE=1 SV=1	F7FJQ3	Npc2
Nuclear ubiquitous casein and cyclin-dependent kinase substrate 1 OS=Rattus norvegicus GN=Nucks1 PE=1 SV=1	Q9EPJ0	Nucks1
Nucleobindin-1 OS=Rattus norvegicus GN=Nucb1 PE=1 SV=1	Q63083	Nucb1

Nucleobindin-2 OS=Rattus norvegicus GN=Nucb2 PE=1 SV=1	Q9JI85	Nucb2
Nucleoside diphosphate kinase A OS=Rattus norvegicus GN=Nme1 PE=1 SV=1	Q05982	^γ Nme1
Nucleoside diphosphate kinase B OS=Rattus norvegicus GN=Nme2 PE=1 SV=1	P19804	^γ Nme2
Olfactomedin-like 2B OS=Rattus norvegicus GN=Olfml2b PE=4 SV=1	D4A0J7	Olfml2b
Olfactomedin-like protein 3 OS=Rattus norvegicus GN=Olfml3 PE=2 SV=2	B0BNI5	Olfml3
Osteoglycin OS=Rattus norvegicus GN=Ogn PE=1 SV=1	D3ZVB7	Ogn
Osteopontin OS=Rattus norvegicus GN=Spp1 PE=1 SV=2	P08721	Spp1
Out at first protein homolog OS=Rattus norvegicus GN=Oaf PE=2 SV=1	Q6AYE5	Oaf
Protein Descriptions	UniProt Accession ID	Gene Symbol
Pappalysin 2 OS=Rattus norvegicus GN=Pappa2 PE=4 SV=2	D3ZQ32	Pappa2
Peptidyl-glycine alpha-amidating monooxygenase OS=Rattus norvegicus GN=Pam PE=1 SV=1	P14925	Pam
Peptidyl-prolyl cis-trans isomerase A OS=Rattus norvegicus GN=Ppia PE=1 SV=2	P10111	Ppia
Peptidyl-prolyl cis-trans isomerase B OS=Rattus norvegicus GN=Ppib PE=1 SV=3	P24368	Ppib
Peptidylprolyl isomerase OS=Rattus norvegicus GN=Fkbp10 PE=1 SV=1	Q5U2V1;A0A096 MJW1	Fkbp10
Periostin OS=Rattus norvegicus GN=Postn PE=1 SV=1	D3ZAF5;A0A097 BW25	Postn
Peroxidasin OS=Rattus norvegicus GN=Pxdn PE=4 SV=1	A0A0G2JWB6	Pxdn
Peroxiredoxin-1 OS=Rattus norvegicus GN=Prdx1 PE=1 SV=1	Q63716	^γ Prdx1
Plasma protease C1 inhibitor OS=Rattus norvegicus GN=Serping1 PE=2 SV=1	Q6P734	^γ Serping1
Plasminogen activator inhibitor 1 OS=Rattus norvegicus GN=Serpine1 PE=2 SV=1	P20961	Serpine1
Platelet-derived growth factor receptor-like protein OS=Rattus norvegicus GN=Pdgfrl PE=2 SV=1	Q5RJP7	^α Pdgfrl
Plexin domain containing 2 OS=Rattus norvegicus GN=Plxdc2 PE=1 SV=1	B5DEZ8	^α Plxdc2
Procollagen C-endopeptidase enhancer 1 OS=Rattus norvegicus GN=Pcolce PE=1 SV=1	O08628	Pcolce
Procollagen-lysine,2-oxoglutarate 5-dioxygenase 1 OS=Rattus norvegicus GN=Plod1 PE=2 SV=1	Q63321	Plod1
Procollagen-lysine,2-oxoglutarate 5-dioxygenase 2 OS=Rattus norvegicus GN=Plod2 PE=2 SV=1	Q811A3	^α Plod2
Procollagen-lysine,2-oxoglutarate 5-dioxygenase 3 OS=Rattus norvegicus GN=Plod3 PE=2 SV=1	Q5U367	Plod3
Profilin-1 OS=Rattus norvegicus GN=Pfn1 PE=1 SV=2	P62963	Pfn1
Pro-neuropeptide Y OS=Rattus norvegicus GN=Npy PE=1 SV=1	P07808	Npy
Prosaposin OS=Rattus norvegicus GN=Psap PE=1 SV=1	P10960;F7EPE0	Psap
Protein CYR61 OS=Rattus norvegicus GN=Cyr61 PE=2 SV=1	Q9ES72	Cyr61
Protein disulfide-isomerase A3 OS=Rattus norvegicus GN=Pdia3 PE=1 SV=2	P11598	Pdia3
Protein NOV homolog OS=Rattus norvegicus GN=Nov PE=1 SV=1	Q9QZQ5	Nov
Protein S100-A11 OS=Rattus norvegicus GN=S100a11 PE=3 SV=1	Q6B345	S100a11

Protein shisa-5 OS=Rattus norvegicus GN=Shisa5 PE=1 SV=1	A0A0G2K447	Shisa5
Protein tyrosine phosphatase receptor type K OS=Rattus norvegicus GN=Ptpk PE=1 SV=1	A5I9F0	Ptpk
Protein tyrosine phosphatase, receptor type, D OS=Rattus norvegicus GN=Ptpd PE=1 SV=2	M0RB22	Ptpd
Protein tyrosine phosphatase, receptor type, G OS=Rattus norvegicus GN=Ptpg PE=1 SV=1	A0A0G2K561	^γ Ptpg
Protein-lysine 6-oxidase OS=Rattus norvegicus GN=Lox PE=1 SV=2	P16636	Lox
Protein Descriptions	UniProt Accession ID	Gene Symbol
Putative uncharacterized protein RGD1565772_predicted OS=Rattus norvegicus GN=Ssc5d PE=4 SV=1	D3ZPK4	Ssc5d
Pyruvate kinase PKM OS=Rattus norvegicus GN=Pkm PE=1 SV=3	P11980	^γ Pkm
Q6AYQ9 Q6AYQ9_RAT	Q6AYQ9	Ppic
RCG41803, isoform CRA_a OS=Rattus norvegicus GN=RT1-N2 PE=3 SV=1	Q6MFZ8	^γ RT1-N2
RCG45259 OS=Rattus norvegicus GN=LOC684828 PE=1 SV=2	M0R7B4	LOC684828
RCG55135, isoform CRA_b OS=Rattus norvegicus GN=Tln1 PE=1 SV=1	G3V852	Tln1
Ribonuclease 4 OS=Rattus norvegicus GN=Rnase4 PE=1 SV=1	O55004	Rnase4
RT1 class I histocompatibility antigen, AA alpha chain OS=Rattus norvegicus PE=1 SV=2	P16391	^γ
RT1 class I, N3 OS=Rattus norvegicus GN=RT1-N3 PE=2 SV=1	Q6MG01	^γ RT1-N3
RT1 class Ia, locus A1 OS=Rattus norvegicus GN=RT1-A1 PE=1 SV=1	A0A0G2K1E1	^γ RT1-A1
Rtf1, Paf1/RNA polymerase II complex component, homolog (S. cerevisiae) OS=Rattus norvegicus GN=Rtf1 PE=1 SV=1	D3ZLH8	^γ Rtf1
Sema domain, immunoglobulin domain (Ig), and GPI membrane anchor, (Semaphorin) 7A (Predicted) OS=Rattus norvegicus GN=Sema7a PE=3 SV=1	D3ZQP6	Sema7a
Semaphorin 3C OS=Rattus norvegicus GN=Sema3c PE=3 SV=1	F7FHT4	Sema3c
Semaphorin 3D OS=Rattus norvegicus GN=Sema3d PE=3 SV=1	F1MAG8	ⁿ Sema3d
Serine (Or cysteine) peptidase inhibitor, clade C (Antithrombin), member 1 OS=Rattus norvegicus GN=Serpinc1 PE=1 SV=1	Q5M7T5	Serpinc1
Serine protease 23 OS=Rattus norvegicus GN=Prss23 PE=4 SV=1	A0A0G2JU46	Prss23
Serine protease HTRA1 OS=Rattus norvegicus GN=Htra1 PE=2 SV=1	Q9QZK5	Htra1
Serpin H1 OS=Rattus norvegicus GN=Serpinh1 PE=1 SV=1	P29457	Serpinh1
Similar to glyceraldehyde-3-phosphate dehydrogenase OS=Rattus norvegicus GN=LOC303448 PE=1 SV=1	Q498M9	^γ LOC303448
Similar to RIKEN cDNA 1300017J02 OS=Rattus norvegicus GN=RGD1310507 PE=1 SV=3	E9PST1;A0A0G2K896	ⁿ RGD1310507
Similar to RT1 class I, CE11 OS=Rattus norvegicus GN=LOC683761 PE=3 SV=3	F1MAQ9	^γ RT1-CE7
Slit homolog 1 protein OS=Rattus norvegicus GN=Slit1 PE=1 SV=1	O88279	^γ Slit1
Slit homolog 2 protein OS=Rattus norvegicus GN=Slit2 PE=4 SV=2	F1MA79	Slit2
SPARC OS=Rattus norvegicus GN=Sparc PE=1 SV=4	P16975	Sparc
SPARC-related modular calcium binding protein 1 OS=Rattus norvegicus GN=Smoc1 PE=1 SV=1	Q6IE50	Smoc1
Protein Descriptions	UniProt Accession ID	Gene Symbol

Sulfhydryl oxidase 1 OS=Rattus norvegicus GN=Qsox1 PE=1 SV=1	Q6IUU3	Qsox1
Sushi domain containing 5 (Predicted) OS=Rattus norvegicus GN=Susd5 PE=4 SV=1	D3ZSC1	Susd5
Sushi repeat-containing protein SRPX2 OS=Rattus norvegicus GN=SrpX2 PE=1 SV=1	B5DF94	ⁿ SrpX2
Sushi, von Willebrand factor type A, EGF and pentraxin domain-containing protein 1 OS=Rattus norvegicus GN=Svep1 PE=1 SV=1	P0C6B8	Svep1
Tenascin C OS=Rattus norvegicus GN=Tnc PE=1 SV=1	A0A0G2K1L0	Tnc
Thrombospondin 2 OS=Rattus norvegicus GN=Thbs2 PE=4 SV=2	D4A2G6	Thbs2
Thrombospondin 3 OS=Rattus norvegicus GN=Thbs3 PE=4 SV=1	A0A0G2JZH3	Thbs3
Transcobalamin-2 OS=Rattus norvegicus GN=Tcn2 PE=2 SV=1	Q9R0D6	Tcn2
Transforming growth factor beta-2 OS=Rattus norvegicus GN=Tgfb2 PE=2 SV=2	Q07257	Tgfb2
Transforming growth factor beta-3 OS=Rattus norvegicus GN=Tgfb3 PE=2 SV=2	Q07258	Tgfb3
Transgelin OS=Rattus norvegicus GN=Tagln PE=1 SV=1	A0A0G2JWK7	Tagln
Transgelin-2 OS=Rattus norvegicus GN=Tagln2 PE=1 SV=1	Q5XFX0	Tagln2
Triosephosphate isomerase OS=Rattus norvegicus GN=Tpi1 PE=1 SV=2	P48500	^γ Tpi1
Tubulointerstitial nephritis antigen-like OS=Rattus norvegicus GN=Tinag11 PE=2 SV=1	Q9EQT5	ⁿ Tinag11
Uncharacterized protein OS=Rattus norvegicus GN=Gm5414 PE=3 SV=1	A0A0G2JUG1	^γ Gm5414
Uncharacterized protein OS=Rattus norvegicus GN=Itih2 PE=1 SV=3	D3ZFH5	Itih2
Uncharacterized protein OS=Rattus norvegicus GN=RGD1559534 PE=4 SV=1	F1M9V3	^γ RGD1559534
Uncharacterized protein OS=Rattus norvegicus GN=RGD1564958 PE=1 SV=1	A0A0G2K8S2	RGD1564958
Uncharacterized protein OS=Rattus norvegicus GN=RT1-CE2 PE=3 SV=3	D3ZQG9;A0A0G2K8R6	^γ RT1-CE2
Uncharacterized protein OS=Rattus norvegicus GN=Thbs1 PE=1 SV=2	M0R979;A0A0G2JV24	Thbs1
Uncharacterized protein OS=Rattus norvegicus PE=1 SV=2	F1M2N4	N/A
Uncharacterized protein OS=Rattus norvegicus PE=1 SV=3	F1LTJ5	N/A
Uncharacterized protein OS=Rattus norvegicus PE=4 SV=3	F1M8C7	N/A
Uncharacterized protein OS=Rattus norvegicus PE=4 SV=3	F1LUI2	N/A
Versican core protein (Fragments) OS=Rattus norvegicus GN=Vcan PE=2 SV=2	Q9ERB4;D3Z9N6	Vcan
Vimentin OS=Rattus norvegicus GN=Vim PE=1 SV=2	P31000	Vim
Vinculin OS=Rattus norvegicus GN=Vcl PE=1 SV=1	P85972	Vcl
Protein Descriptions	UniProt Accession ID	Gene Symbol
Vitamin K-dependent protein S OS=Rattus norvegicus GN=Pros1 PE=2 SV=1	P53813	Pros1
V-type proton ATPase subunit S1 OS=Rattus norvegicus GN=Atp6ap1 PE=2 SV=1	O54715	Atp6ap1

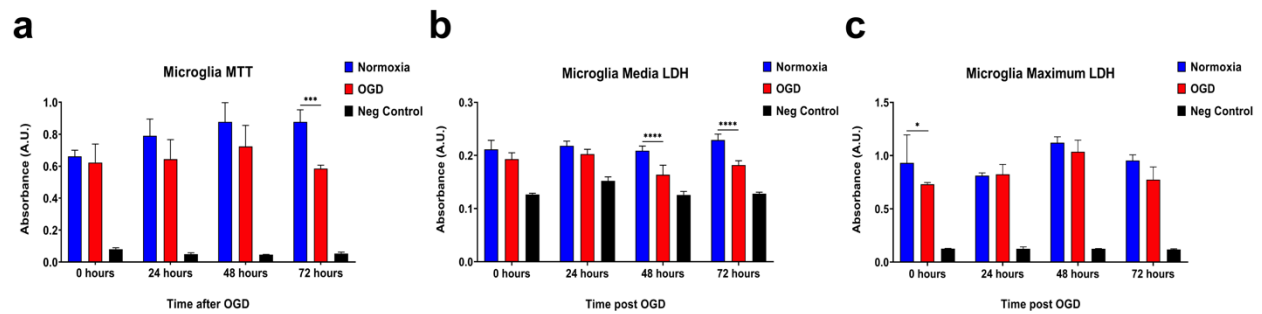
Gene symbols marked with n denote proteins unique to nMSC, gene symbols marked with γ denote proteins unique to aMSC γ .

Table S4. Metacore Pathway Enrichment.

	Pathway	FDR	Network Objects		
			Pathway Total	In Data	Object Name
1	TGF-beta-induced fibroblast/myofibroblast migration and extracellular matrix production in asthmatic airways	0.0001	35	3	Tenascin-C, TGF-beta 3, COL1A2, Collagen IV, Thrombospondin 2
2	Alternative complement cascade disruption in age-related macular degeneration	0.0054	38	3	Factor Ba, Factor Bb, Factor B
3	Development: TGF-beta-dependent induction of EMT via SMADs	0.0054	42	3	TGF-beta, Vimentin, TGF-beta 3
4	WNT signaling in invasive-type melanoma cells	0.0054	47	3	Vimentin, Filamin A, Filamin-A (CTF)
5	Stromal-epithelial interaction in Prostate Cancer	0.0058	48	3	Tenascin-C, Vimentin, TGF-beta 3
6	Development: TGF-beta-dependent induction of EMT via MAPK	0.0058	50	3	TGF-beta, Vimentin, TGF-beta 3
7	Stimulation of TGF-beta signaling in lung cancer	0.0058	53	3	TGF-beta, Vimentin, TGF-beta 3
8	Immune response: Lectin induced complement pathway	0.0058	53	3	C2b, C2a, C2
9	Immune response: Classical complement pathway	0.0058	19	2	C2b, C2a, C2
10	Immune response: Alternative complement pathway	0.0058	25	2	Factor Ba, Factor Bb, Factor B
11	Stem cells Schema: Adult neurogenesis in the Subventricular Zone	0.0158	26	2	Vimentin, CSPG4 (NG2)
12	Immune escape mechanisms in Prostate Cancer	0.0251	28	2	Beta-2-microglobulin, TGF-beta
13	Stem cells: Hypothetical role of microRNAs in fibrosis development after myocardial infarction	0.0251	35	2	Fibrillin 1, COL1A2
14	Tumor-stroma interactions in pancreatic cancer	0.0270	35	2	COL1A2, Thrombospondin 2
15	Production and activation of TGF-beta in airway smooth muscle cells	0.0364	38	2	TGF-beta, TGF-beta 3
16	Role of adhesion of SCLC cells in tumor progression	0.0364	38	2	Tenascin-C, Collagen IV
17	Cell adhesion: Cell-matrix glycoconjugates	0.0364	38	2	Tenascin-C, CSPG4 (NG2)
18	Stem cells: Role of TGF-beta 1 in fibrosis development after myocardial infarction	0.0364	44	2	Tenascin-C, COL1A2
	Pathway	FDR	Network Objects		
			Pathway Total	In Data	Network Objects
19	Development: Neural stem cell lineage commitment (schema)	0.0364	45	2	Vimentin, CSPG4 (NG2)
20	TGF-beta 1-mediated induction of EMT in normal and asthmatic airway epithelium	0.0456	46	2	Tenascin-C, Vimentin

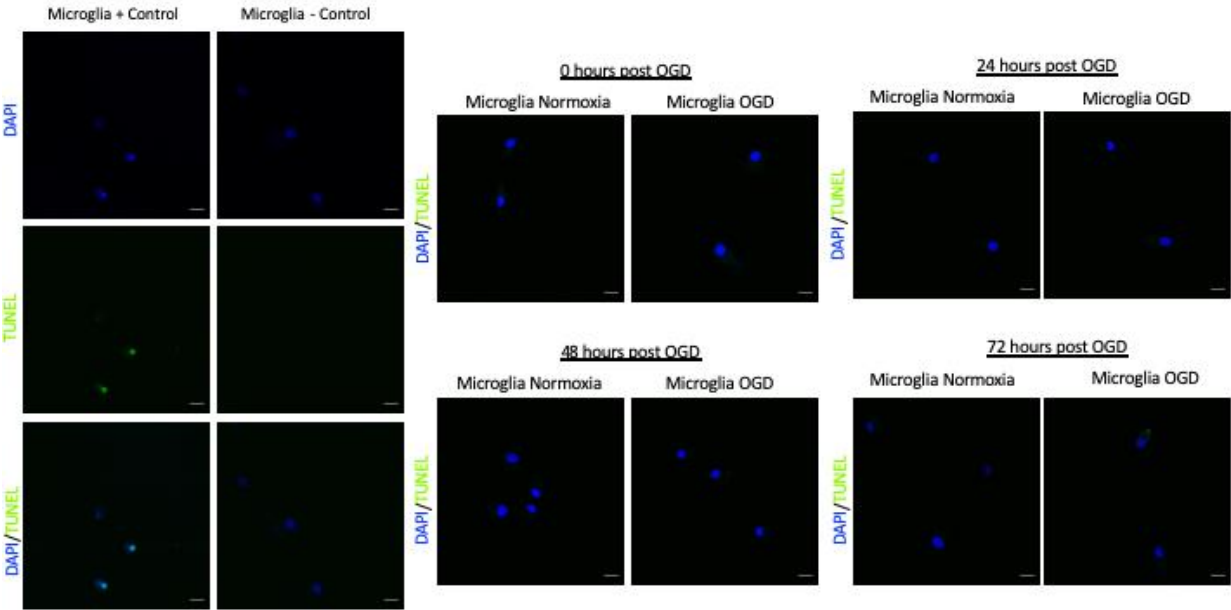
21	LKB1 signaling pathway in lung cancer cells	0.0456	49	2	Vimentin, Collagen IV
22	Development: TGF-beta-dependent induction of EMT via RhoA, PI3K and ILK	0.0456	50	2	Vimentin, TGF-beta 3
23	Cytoskeleton remodeling: Integrin outside-in signaling	0.0491	35	3	Filamin A, Collagen IV
24	Immune response_IL-13 signaling via PI3K-ERK pathway	0.0491	38	3	Tenascin-C, COL1A2

Figure S1. Microglia viability studies after oxygen glucose deprivation (OGD) conditions.



(a) Microglia 3-(4,5-Dimethylthiazol-2-Yl)-2,5-Diphenyltetrazolium Bromide (MTT) assay after OGD. **(b)** Microglia release of lactate dehydrogenase (LDH) in media after OGD. **(c)** Microglia maximum LDH from cell lysate after OGD. Data were analyzed using two-way ANOVA with Tukey multiple comparison testing. * $p \leq 0.05$, *** $p < 0.001$, **** $p < 0.0001$.

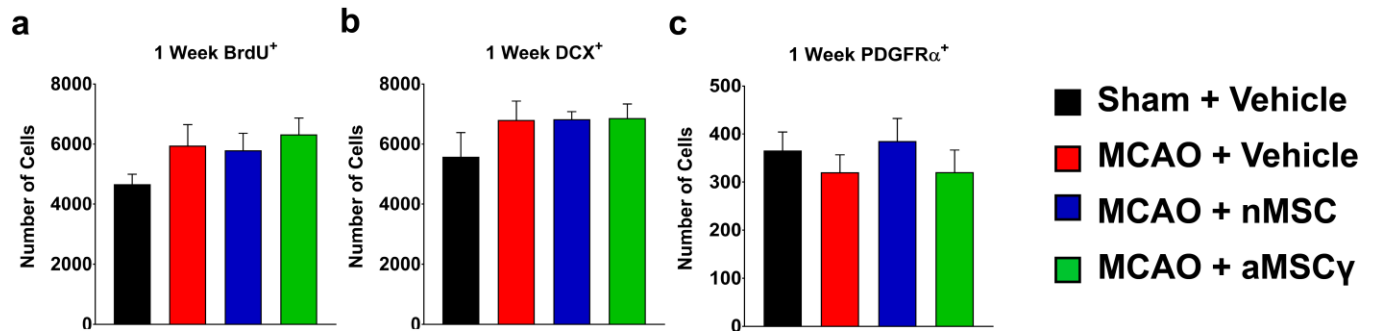
Figure S2. Microglia TUNEL Assay after oxygen glucose deprivation (OGD).



(a) Representative confocal images of Microglia positive and negative controls. **(b)**

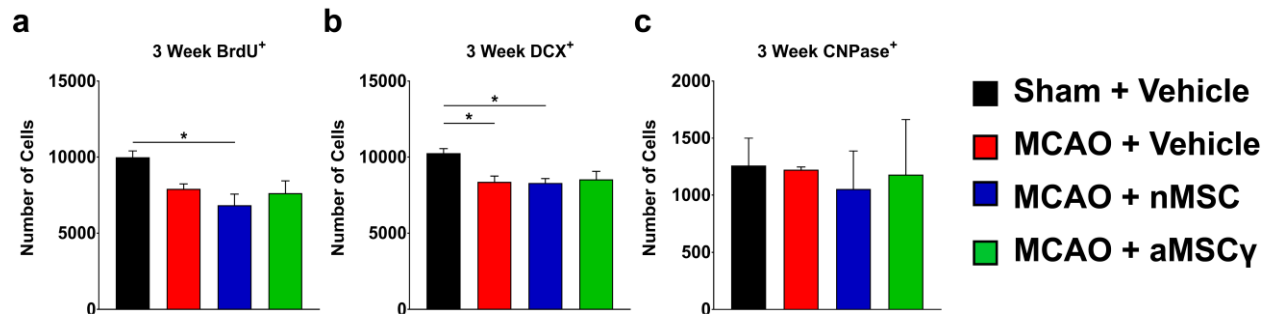
Representative confocal images of Microglia after OGD. DAPI (blue), SA-488 (green). Scale bar 10 μm .

Figure S3. Changes in subventricular zone (SVZ) composition at 1 week after MCAO.



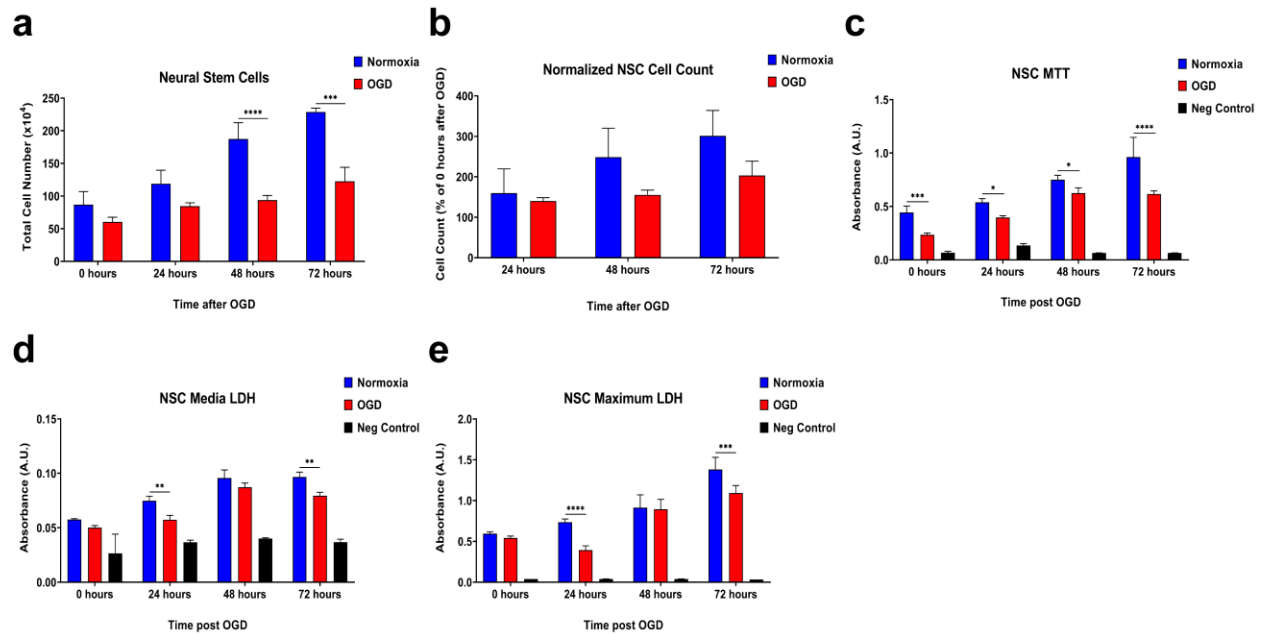
(a) Bromodeoxyuridine (BrdU)⁺ cell counts in the SVZ. (b) Doublecortin (DCX)⁺ cell counts in the SVZ. (c) Platelet derived growth factor receptor alpha (PDGFR α)⁺ cell counts in the SVZ. Data are mean \pm S.E.M.; n = 3 animals for sham + vehicle group, n = 5-6 for the remaining groups. Data were analyzed using nonparametric Kruskal-Wallis one-way ANOVA.

Figure S4. Changes in subventricular zone (SVZ) composition at 3 weeks after middle cerebral artery occlusion (MCAO).



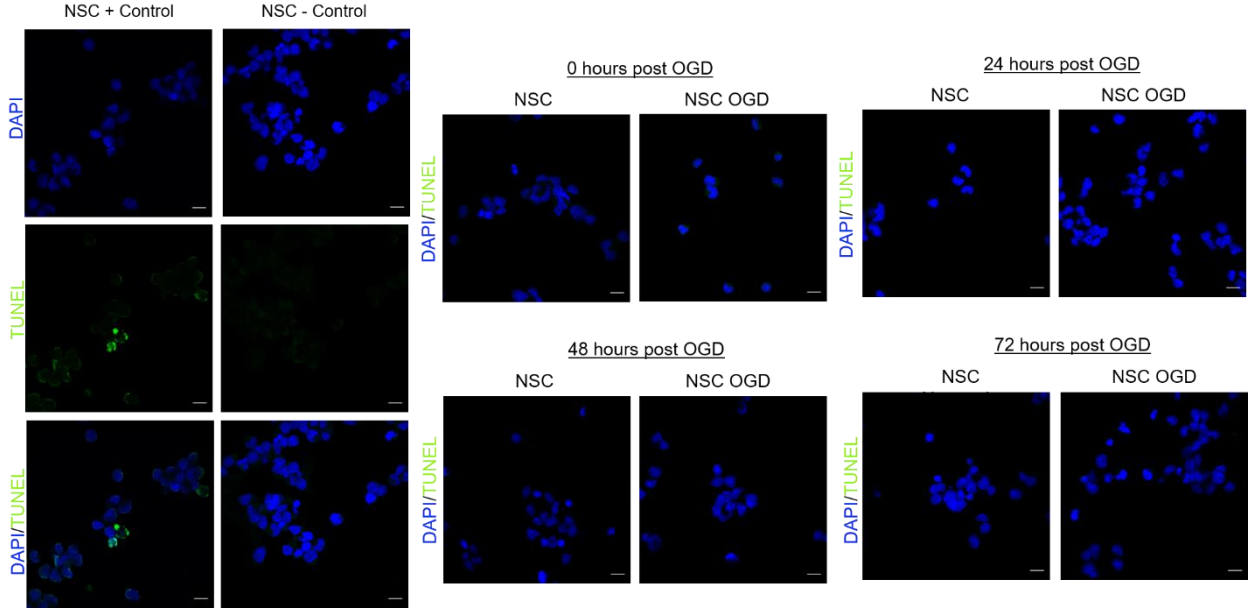
(a) Bromodeoxyuridine (BrdU)⁺ cell counts in the SVZ. (b) Doublecortin (DCX)⁺ cell counts in the SVZ. (c) 2'3'-Cyclic-nucleotide 3'phosphodiesterase (CNPase⁺) cell counts in the SVZ. Data are mean ± S.E.M.; n = 3 animals per group. Data were analyzed using nonparametric Kruskal-Wallis one-way ANOVA. *p≤0.05.

Figure S5. Neural stem cell (NSC) viability studies after oxygen glucose deprivation (OGD) conditions.



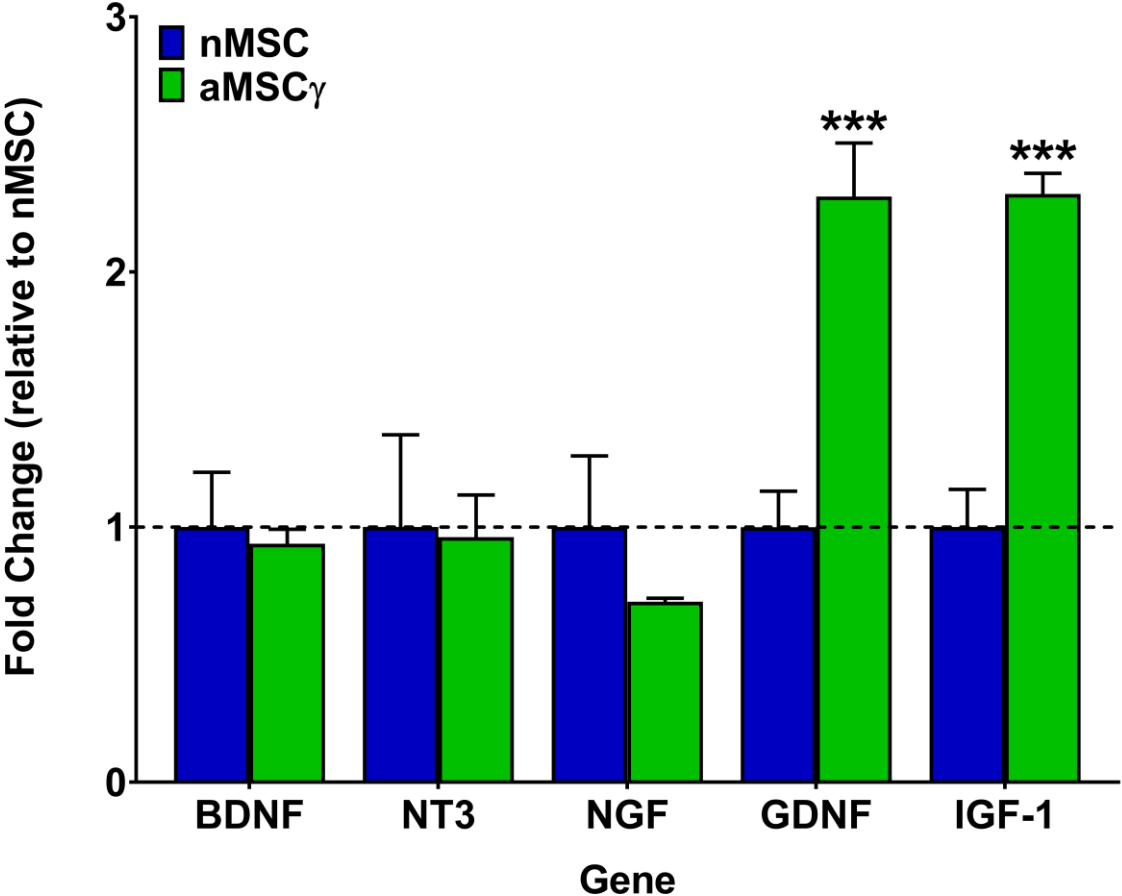
(a) NSC cell counts after OGD. (b) NSC cell counts normalized to 0 hours post OGD. (c) NSC 3-(4,5-Dimethylthiazol-2-Yl)-2,5-Diphenyltetrazolium Bromide (MTT) assay after OGD. (d) NSC release of lactate dehydrogenase (LDH) in media after OGD. (e) NSC maximum LDH from cell lysate after OGD. Data were analyzed using two-way ANOVA with Tukey multiple comparison testing. * $p \leq 0.03$, ** $p \leq 0.002$, *** $p \leq 0.0002$, **** $p \leq 0.0001$

Figure S6. Neural stem cell (NSC) TUNel Assay after oxygen glucose deprivation (OGD).



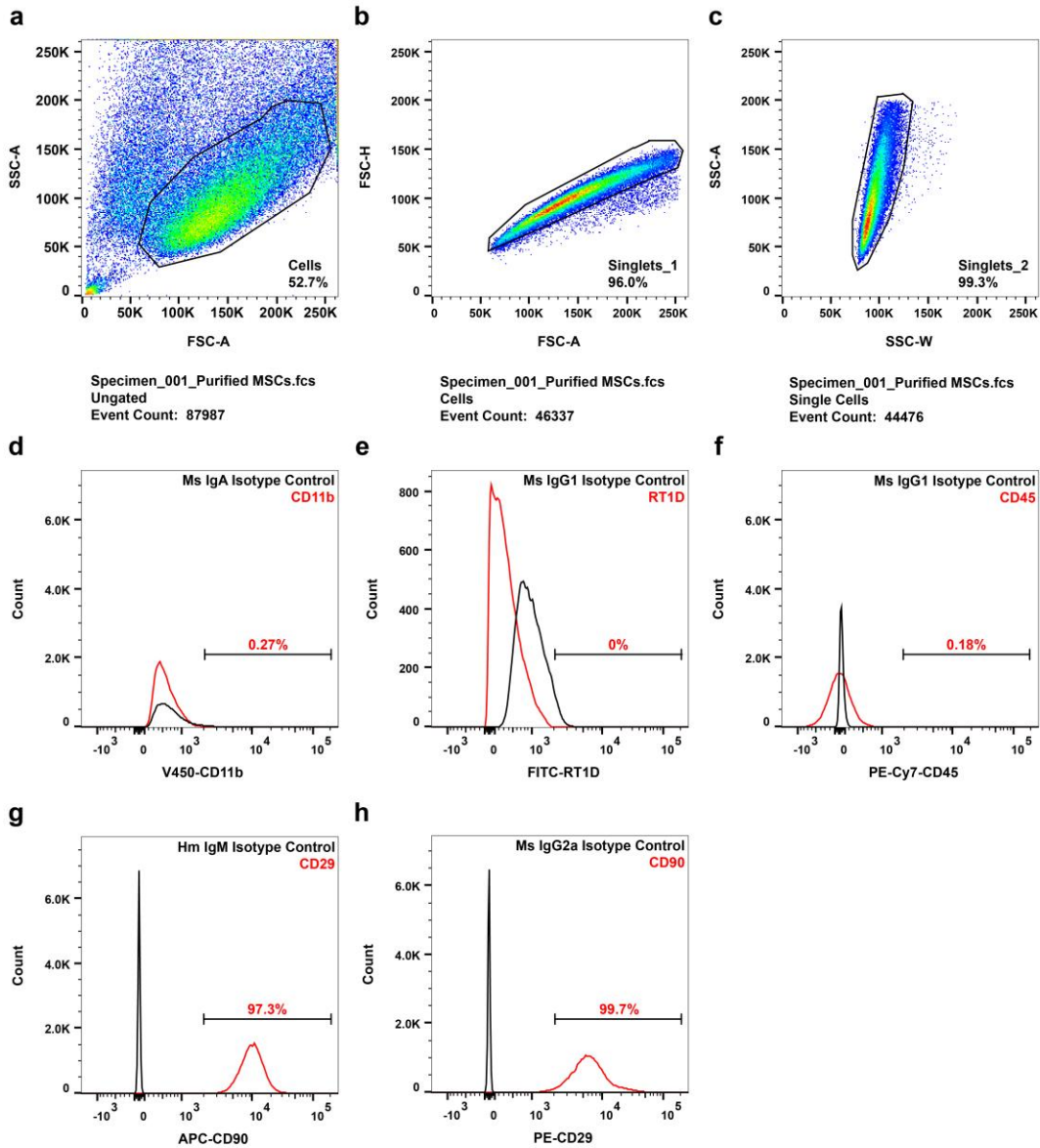
(a) Representative confocal images of NSC positive and negative controls. **(b)** Representative confocal images of NSC after OGD. DAPI (blue), SA-488 (green). Scale bar 10 μ m

Figure S7. Neurotrophic factor expression by mesenchylam stem cells (MSCs).



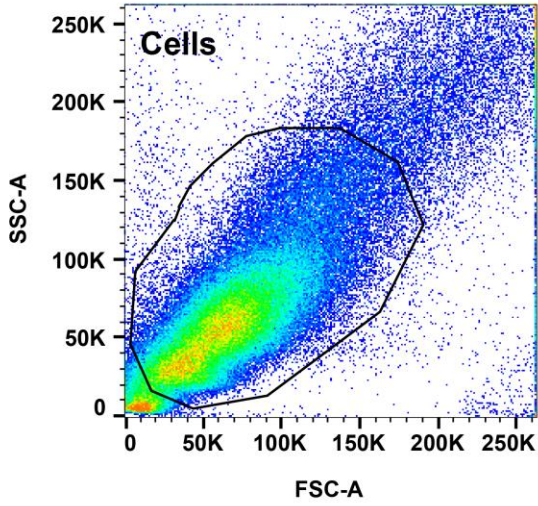
mRNA levels of brain derived neurotrophic factor (BDNF), neurotrophin 3 (NT3), nerve growth factor (NGF), glial derived neurotrophic factor (GDNF), and insulin growth factor 1 (IGF-1) from nMSC and aMSC γ . Data are mean \pm S.E.M.; n = 3 independent experiments. Data were analyzed by two-tail unpaired t-test. ***p<0.001.

Figure S8. Mesenchymal stem cell (MSC) surface marker analysis.

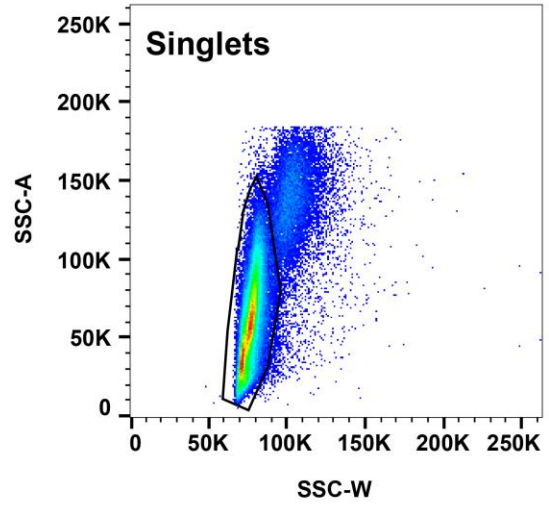


(a-c) Flow cytometry gating strategy. (d-h) MSC surface marker (red lines on histograms) expression CD11b (d), RT1D (e), CD45 (f), CD29 (g), CD90 (h), and corresponding isotype controls (black lines on histograms).

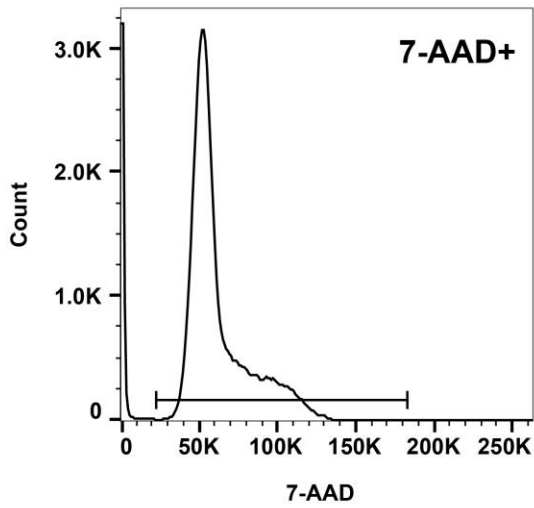
Figure S9. Gating strategy for BrdU flow cytometry.



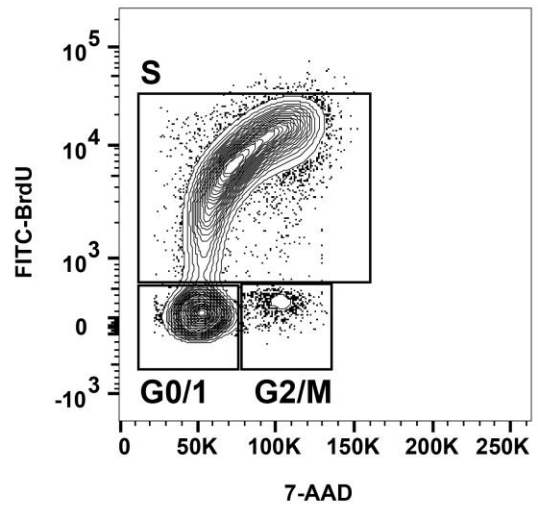
Specimen_001_24 NCM 1.fcs
Ungated
Event Count: 158392



Specimen_001_24 NCM 1.fcs
Cells
Event Count: 113968



Specimen_001_24 NCM 1.fcs
Single Cells
Event Count: 101832



Specimen_001_24 NCM 1.fcs
DNA BrdU gated
Event Count: 69410

Supplemental Video Legend:

Video S1. T2-weighted magnetic resonance (MR) imaging from middle cerebral artery occlusion (MCAO) animals. Left panel is vehicle treated, middle panel is naïve mesenchymal stem cells (nMSC) treated, and right panel is aMSC γ treated animals. Best viewed with Windows Media Player.